

COVELL, ALAN D., Ph.D. At The Interface: Biotic-Abiotic Interactions Between Substrates and A Model Epithelium. (2015)
Directed by Dr. Dennis LaJeunesse. 123 pp.

The need for determining the fundamental mechanisms that define the interaction of biological systems with underlying materials, both natural and synthetic, is important as humanity endeavors to improve the quality of life of individuals through technology. Recently, much work has focused on the role of material properties on the behavior of cells. Most of these studies have concentrated their efforts on fibroblastic cell lines and more recently different kinds of stem cells. While these cells represent an important subset of cells in complex organisms, they do not manifest cell-cell interactions, a feature of epithelial cells, the most abundant cell type. Epithelial cells represent the largest cell type in the body and introduce an intrinsic complexity when researching the interaction of biological systems with materials. Adherens junctions (AJ) play a significant role in many signaling pathways, and therefore there is need to investigate how physical interactions with underlying substrates affect cell-cell interactions, such as the adhesion properties between cells, as well as how cell-substrate interactions influence the morphology and growth of epithelial cells. In this work I seek to determine the effects and identify mechanisms that epithelial cells use to “read” their environment. To do this I examined changes in cell behavior (growth, morphological, adhesion) of a model epithelium on substrates that have similar composition but significant differences in surface organization.

In such a manner, I probed the limitations at which the nanoscale differences in substrate topography affect cellular behavior.

AT THE INTERFACE: BIOTIC-ABIOTIC INTERACTIONS BETWEEN
SUBSTRATES AND A MODEL EPITHELIUM

by

Alan D. Covell

A Dissertation Submitted to
the Faculty of The Graduate School at
The University of North Carolina at Greensboro
in Partial Fulfillment
of the Requirements for the Degree
Doctor of Philosophy

Greensboro
2015

Approved by

Committee Chair

APPROVAL PAGE

This dissertation written by ALAN D. COVELL has been approved by the following committee of the Faculty of The Graduate School at The University of North Carolina at Greensboro.

Committee Chair

Dennis LaJeunesse

Committee Members

Daniel Herr

Chris Kepley

Promod Pratap

Date of Acceptance by Committee

Date of Final Oral Examination

TABLE OF CONTENTS

	Page
LIST OF TABLES	v
LIST OF FIGURES	vi
CHAPTER	
I. INTRODUCTION	1
II. LITERATURE REVIEW	5
II.1 Fundamentals of an Epithelial Cell	6
II.2 Cellular Adhesion Mechanisms	8
II.2.i Non-specific Adhesion	8
II.2.ii Cell-Substrate Adhesion: Integrins	12
II.2.iii Cell-Cell Adhesion: Adherens Junctions	16
II.3 Adhesion On Engineered Substrates	19
II.3.i Protein Adsorption.....	19
II.3.ii Nanoscale Influences on Cellular Behavior.....	23
II.4 Probing the Mechanical Properties of Cells.....	27
II.4.i Cells as Viscoelastic Materials.....	27
II.4.ii Basics of Atomic Force Microscopy	29
II.4.iii Force Modulation Microscopy for Studying Biological Samples.....	35
II.5 Summary	39
III. INVESTIGATING THE LOWER LIMITS OF THE EFFECT OF NANOTOPOGRAPHY	41
III.1 Introduction	41
III.2 Materials and Methods	43
III.3 Results	44
III.4 Discussion/Conclusion.....	52
IV. DIFFERENT CRYSTALLINE STRUCTURES DRIVE VARIATIONS IN ECM COMPOSITION AND MORPHOLOGY	55
IV.1 Introduction.....	55
IV.2 Materials and Methods.....	57
IV.3 Results	60
IV.4 Discussion/Conclusion	82

V. AFM FOR THE INVESTIGATION OF DYNAMIC BIOLOGICAL SYSTEMS	86
V.1 Introduction.....	86
V.2 Materials and Methods	88
V.3 Results	90
V.4 Discussion/Conclusion	97
VI. CONCLUSION AND GUIDING PRINCIPLES	100
REFERENCES	104
APPENDIX A. EXPANDED FIGURE.....	114

LIST OF TABLES

	Page
Table 3.1. Island Organization at a Low Starting Concentration of Cells.....	50
Table 4.1. Morphology and Growth Habit of MDCK Cells on GCS, <111>, and <100> Substrates.	68
Table 4.2. Basal F-Actin and Adherens Junction Organization in MDCK Cells Cultured on Glass and Si Wafers.....	72

LIST OF FIGURES

	Page
Figure 1.1. PLLA/PS Nanotopographies.....	3
Figure 2.1. Interests of Investigation.....	6
Figure 2.2. Fundamental Parts of an Epithelial Cell.....	7
Figure 2.3. Basic Interactions of Biological Systems with Materials.	11
Figure 2.4. Overview of Initial Adhesion and FA Maturation.	14
Figure 2.5. Overall Structure of the E-Cadherin Complex.	17
Figure 2.6. Stress and Strain.....	28
Figure 2.7. Modes of Operation in the AFM.....	31
Figure 2.8. Simple AFM Setup.....	33
Figure 2.9. Force Modulation Microscopy with the AFM.....	36
Figure 3.1. AFM Images of the Topography of the Glass and Si Wafer Substrate Used in this Study.....	45
Figure 3.2. Growth of MDCK and NIN3T3 Cells on Glass and Si Wafer with “Low” Concentration of Cells.	47
Figure 3.3. Growth of MDCK and NIH3T3 Cells on Glass and Si Wafer with “High” Concentration of Cells.	48
Figure 3.4. Preferential “Island” Growth of Epithelial Cells	49
Figure 3.5. Morphology and F-actin Localization in Cells Grown on Glass and Si Wafer Plated Under “Low” Cell Concentration.....	51
Figure 4.1. Atomic Force Micrographs of GCS, <111>, and <100> Substrates Used in this Study.....	61
Figure 4.2. Statistical Significance Between All Surfaces Used.....	62
Figure 4.3. Epithelial Cell Growth on GCS, <111>, and <100> Silicon.....	66

Figure 4.4. Confocal Micrographs Demonstrating the Growth Habit and Morphology of MDCK Cells Cultured on GCS and Si Wafers, <111> and <100>.....	67
Figure 4.5. AFM Force Amplitude Images of MDCK Cells Cultured on GCS, <111> and <100> Substrates.....	69
Figure 4.6. Cell Wash Assay on MDCK Cells Cultured on GCS, <111> and <100> Substrates.	71
Figure 4.7. Basal Actin and Adherens Junction Organization in MDCK Cells	73
Figure 4.8. Chemiluminescent Surface Analysis of ECM Protein Adsorption on GCS, <111>, and <100> Substrates.....	76
Figure 4.9. AFM Analysis of ECM Protein Aggregates Adsorbed on GCS, <111>, and <100> Substrates.....	78
Figure 4.10. ECM Protein Expression Levels in MDCK Cells Cultured on GCS, <111>, and <100> Substrates.....	80
Figure 4.11. Fibronectin Expression in MDCK Epithelial Cells Cultured on GCS, <111> and <100> Substrates.....	81
Figure 5.1. Typical Force Distance Curve Using the AFM.....	87
Figure 5.2. Deflection Images of MDCK Cells on Various SiO ₂ Substrates.....	91
Figure 5.3. Profiles of FMM AFM Image of MDCK Cells on GCS.....	93
Figure 5.4. FMM Amplitudes On and Off the Cell.....	94
Figure 5.5. Phase Profiles of Each Surface.....	96
Figure A1. Bar Graph Representation of MDCK Cell Growth Rate.....	114

CHAPTER I

INTRODUCTION

Medical technology has seen incredible advancements in the last century. Innovations such as magnetic resonance imaging (MRI), along with innovative dyes, allow for incredibly safe and high resolution visualization and diagnosis [1, 2]. Nanotechnology holds the possibility of improving these technologies further. The manipulation of nanoscale materials such as nanovesicles and fullerenes hold the potential to offer new ways to treat and diagnosis various diseases [3-5]. For example, nanovesicles have been used as targeted treatments for glioblastoma. Nanovesicles of 104 nm were conjugated with human interleukin-13 protein to specifically target malignant cancer cells. Conjugated vesicles were shown to have a 5 fold greater reduction in tumor size compared to controls [6]. Manipulating the organization or structure of substrates at the nanoscale has also demonstrated improvements to current technology, such as implantable devices. This nanotopography has demonstrated promise in controlling cell fate and function [7], having the potential to grow entire organs [8]. While much research has been focused on several aspects of these materials and their potential uses, many of the fundamental rules governing the interactions between cell and extracellular materials, both natural and synthetic, are not entirely understood [9]. For example, grooves can influence the polarity of cells. PC12

cells were cultured on grooves with widths of 500-2000 nm, where widths were varied at 250 nm intervals and all groove sizes had depths of 350 nm. Groove widths of 500-1000 nm showed a selection for bipolar cells, where grooves greater than 1250 nm selected for multipolar cells. The mechanism behind this selection seemed to be related to the formation and structure of focal adhesion complexes (FAC) [10].

This cell-substrate phenomenon has been explained by the concept of contact guidance [9-11]. The concept of contact guidance was first introduced in the sixties. The idea is that the physical restriction of the cell forces growth, or migration, in a certain direction due to no other path being available [11]. While the original concept of contact guidance involved macro and microscopic grooves, the same phenomenon can be observed with nanostructured materials [9-11]. Such an example suggests that FAC are essential for observed effects on nanotopography. [12, 13]. However, nanotopographies can influence more than simple FAC formation and maturation. As an example see Figure 1.1; the phase separation of PLLA/PS solutions during spin casting created well defined nanotopographies.

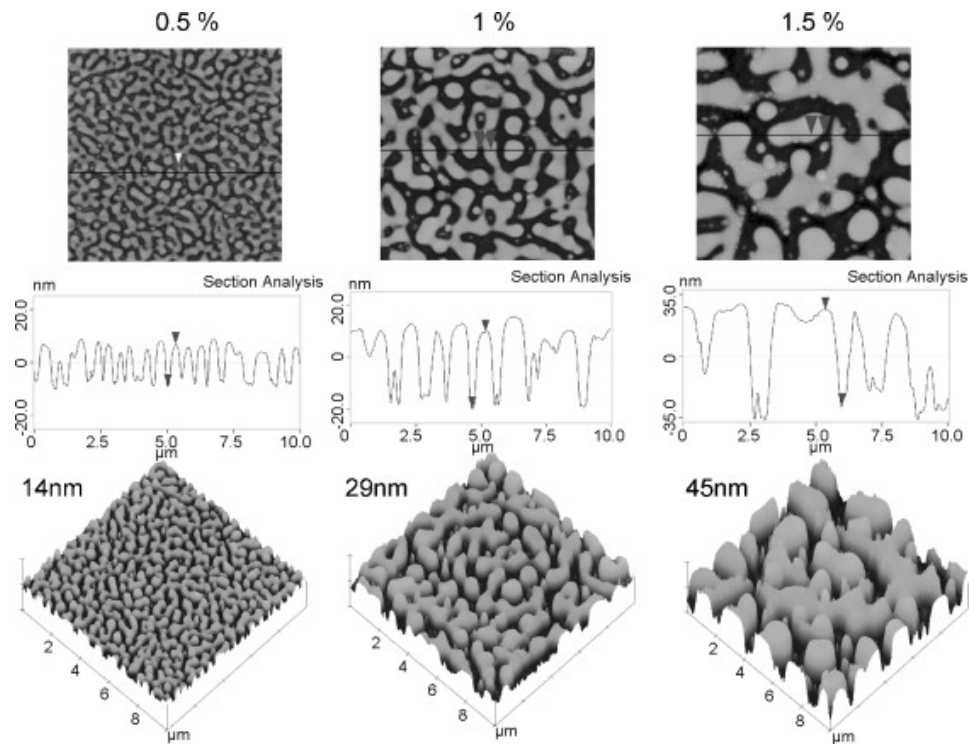


Figure 1.1. PLLA/PS Nanotopographies.

AFM images for the PLLA/PS (50/50, w/w) demixed nanotopographies as obtained after spin casting from solutions of concentrations 0.5, 1 and 1.5 wt% in chloroform. The first row shows the height magnitude, the second one the transversal cut and the last one the 3D reconstruction of the surface [14].

MC3T3 osteoblast-like cells were cultured on each surface. Cellular adhesion, protein adsorption and organization were examined. Cells adhered to all topographies similarly. However, 14 nm topographies demonstrated increased protein adsorption overall compared to the 29, and 45 nm topographies. Also, cells demonstrated various behaviors in vinculin organization, FAC size, and fibronectin matrix reorganization on 14 nm compared to the 29, and 45 nm topographies. This suggests nanotopography can have a more subtle effect than simple morphological changes or determining where cells form FACs [14].

Studies such as this demonstrate how nanotopography can influence cellular behavior, but raise questions regarding the specific nature of influence of nanotopography at the interface of biotic and abiotic materials. Questions remain, such as what the size/scale limits are for nanotopographies to influence cellular behavior. For instance, fibroblasts interact with nanofeatures as small as 10 nm, where EM images show filipodia attached to the small nanopillars [11]. However these experiments provide little more than a demonstration of a cell's contact with such structures and do not show whether these filopodial contacts provide information that results in meaningful changes to the state of the cell; i.e. change in morphology, growth or differentiation. It may be unlikely that cells directly interact with features smaller than this due to various spatial restrictions that are inherent in cells building meaningful adhesion complexes [15], although substrates ordered at smaller sizes (<10 nm) may have an indirect effect, for example by influencing the organization of proteins in the ECM . [16, 17].

In order to fully understand the possibilities technologies such as nanotopography may provide a better understanding of the fundamental rules governing the interactions of cells with the interface of these materials is needed. The goal of my research is to determine the limit that topographical changes affect cellular behavior, define the responses of cells to these changes and identify the mechanisms that cells use to read the variations in such substrates. Additionally, I characterize the mechanical differences of the cells on the substrates and develop techniques to study mechanical properties of cells.

CHAPTER II

LITERATURE REVIEW

In this work, I have investigated some of the fundamental rules that govern the interaction of biological systems with non-biological materials. I examined the limitations at which nanoscale variations of surface structure can affect cell behavior, I also investigated how the cell is able to "read" the surface and compensate for those differences, and examined how the mechanical properties of the cell change in relation to different substrates. I've chosen to use a model epithelial cell line, Madin-Darby Canine Kidney (MDCK) cells, because epithelial cells are an underrepresented cell type in the literature but represent an important and abundant cell type in mammals. Unlike mesenchymal cells, epithelial cells have a second complex adhesion system in cell-cell mediated adhesion. First, I will cover what makes epithelial cells unique, providing background of the necessary cell biology. Second, I will also cover known adhesion mechanisms, both non-specific elements, as well as molecular elements the cell uses specifically, namely integrins and adherens junctions, to provide background for interpreting results and providing context for further questions. Third, I will then look at nanoscale engineered materials in order to provide context for the work in this study and how it may be applicable in the broader field. And finally, I will examine the tools used to investigate the

mechanical properties of cells and the background necessary in order to develop new tools and techniques to answer further questions in following research.

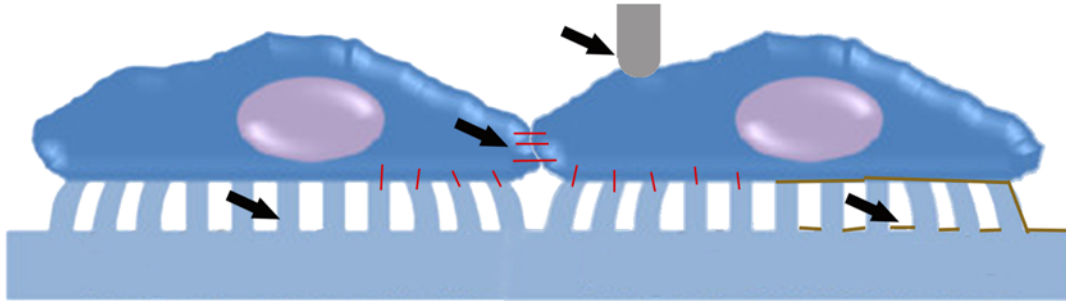


Figure 2.1. Interests of Investigation.

We are interested two specific kinds of adhesion, cell-cell adhesion via e-cadherin, and cell-matrix adhesion via integrins. Also, note the interaction of both the cell and adsorbed protein with the substrate. And finally, we pursue methods to probe the mechanical properties of the cell via Atomic Force Microscopy (AFM), using Force Modulation Microscopy (FMM).

II.1 Fundamentals of an Epithelial Cell

Epithelial cells are sheets of cells that function in many roles; epithelial cells serve as a fundamental cell type in the development of almost all tissues. In adults, epithelial cells serve as barriers between the external and internal portions of the organism as well as line organs and cavities inside the body [18]. Epithelia are essential for multicellular organisms because they organize tissue, creating boundaries between organs, and allowing specific transport of molecules, such as oxygen through the lungs. Epithelial cells typically have a very distinct polarity, an apical and basal (top and bottom) orientation. These cells are held together by a series of different junctions. Some characteristic cell-cell interactions that are created and managed in epithelial cells are: occluding

junctions, adherens junctions, desmosomes, and channel-forming junctions (Figure 2.2).

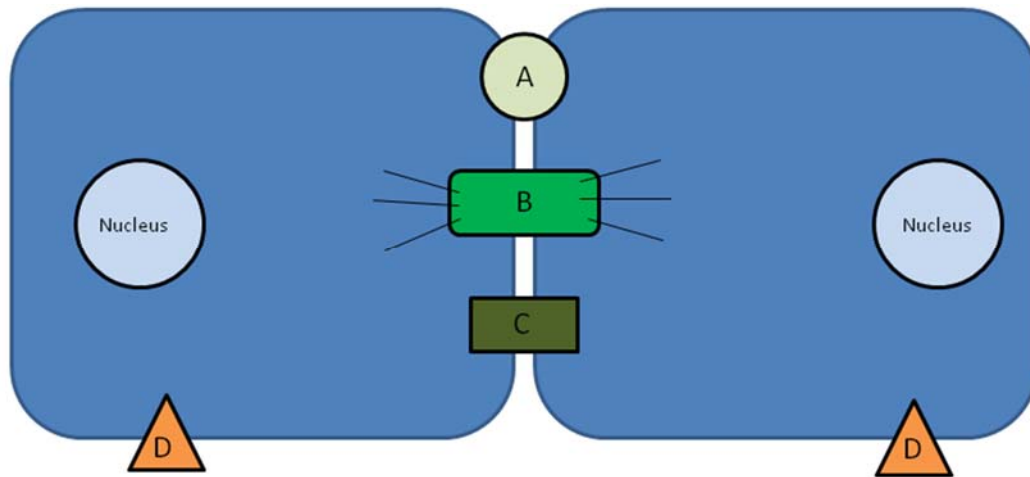


Figure 2.2. Fundamental Parts of an Epithelial Cell. (A) Occluding junctions (tight junctions) (B) Adherens junctions and desmosomes. The dynamic, interlocking mechanism in epithelial cells giving tissue structure and organization. (C) Channel forming junctions. (D) Hemidesmosomes and Focal adhesion complexes.

Occluding junctions or tight junctions are responsible for preventing leakage through the epithelium. These junctions are closest to the apical part of the epithelium. Basal to occluding junctions are the adherens junctions, which function as the major cell-cell adhesion complex in epithelial cells by not only physically linking two cells but also linking their actin cytoskeletons. The cadherin superfamily of proteins are the critical extracellular adhesion molecule found in adherens junctions. The cadherin mediated cell-cell junction participates in several signaling events and is a crucial set of proteins when considering how the cell is interacting with its environment. Desmosomes are the next set of

intercellular interactions that link intermediate filaments of one cell to another. These complexes give the epithelium structural integrity, enabling the organized tissue to resist forces acting on them, such as shear stress. The last set of junctions that are typical are channel-forming junctions. These specific junctions play an important role in that they allow nutrients and other essential molecules to pass laterally through an epithelium. The interplay between each of these different kinds of junctions, what each role means to overall tissue health and operation, is complex. And one must appreciate this complexity, especially when making generalized assertions about the bio-material interface.

11.2 Cellular Adhesion Mechanisms

Three adhesion mechanisms are considered for this work, non-specific adhesion (e.g., electrostatic interactions), cell-substrate adhesion as mediated by integrins, and cell-cell adhesion, mediated by cadherin interactions at the adherens junctions. This not a comprehensive list, but comprise the main components of mechanisms considered in this work.

11.2.i Non-specific Adhesion

The interface of biological to non-biological material is an extremely complex. There are a large number of variables to consider, such as many different cell surface proteins that the cell uses for adhesion, ionic concentrations that will alter local electrostatic fields, inherent charge of materials and proteins, external (and internal) forces, and properties of lipid bilayers (Figure 2.3). [19]

Therefore, there is an interplay of many different force regimes that needed to be considered.

Electrostatic interactions are the largest adhesion force besides biologically specific adhesion protein-ligand binding. Cells themselves will have a charge on the surface of the plasma membrane, this is called the stern layer; the surface charge of a cell is inherent in the composition of the phospholipid bilayer, and to a lesser extent in the exposed protein domains of surface protein, which carry a local charge. However, physiological conditions have a large amount of specific ions that form an electrostatic double layer, the stern layer [19].

According to the Derjaguin and Landau, Verwey and Overbeek (DLVO) theory, the electrostatic double-layer will create a repulsion regime that one might expect to hinder specific binding of cells to surfaces, though it is sensitive to temperature, ionic concentration, and pH. However, this repulsion regime can be overcome by the presence of Ca^{2+} , Mg^{2+} cations, as divalent cations are known to reduce the repulsion regime [19]. These ions are always present in physiological conditions, and specific ions play important roles in various adhesion structures. So, when biological systems are introduced into a physiologically relevant solution an electrostatic double-layer is formed on the cell itself. The ionic layer that surrounds the cell will then interact with the ionic layer present on the surface of whatever substrate is present.

The substrate surface will suffer from the same electrostatic double layer that covers cells. A layer of co-ions and counter-ions are adsorbed onto the

surface, along with ECM proteins, glycol-proteins, and other biological molecules that adhere due to both electrostatic forces as well as van der Waals forces. These interactions form a layer that “biofouls” the surface, allowing for specific biomolecule-ligand adhesion. In physiological conditions, the surface is conditioned in a manner that promotes adhesion, and preventing, or promoting this is a topic of considerable research.

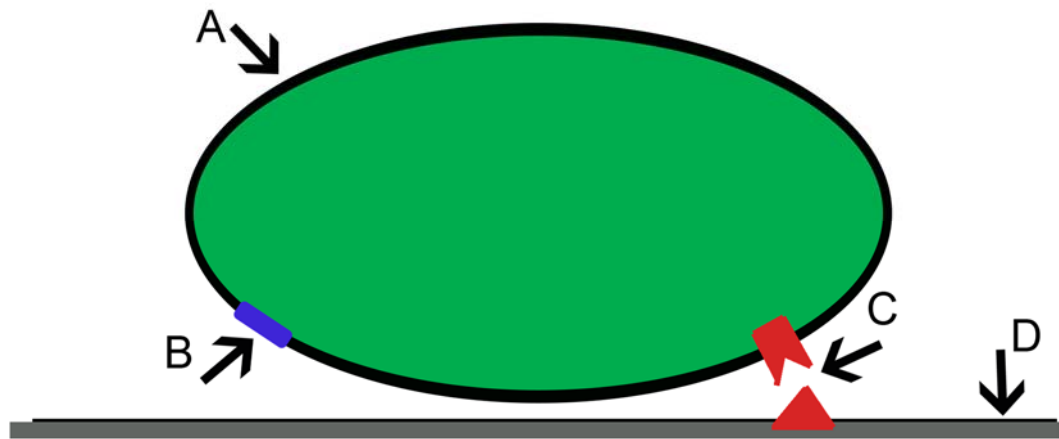


Figure 2.3. Basic Interactions of Biological Systems with Materials.

The green oval represents a cell. (A,D) Represent the charged double layer that will form in the presence of ionic compounds. Because physiological systems contain required Na, K, etc. this is the first layer of contamination that will occur.

(B) represents lipid rafts and other transmembrane proteins that are on the surface of the cell and carry an intrinsic charge that could contribute to local binding at the nanoscale. These specific interactions will not be permanent as the cell is continuously recycling such proteins. (C) represents specific protein-ligand interactions. These are normal adhesion events in situ; they can be mimicked in this case as several ECM proteins are present in any culture medium of physiologically relevant conditions, hence those proteins may adsorb and provide adhesion points.

Overall, electrostatic interactions along with van der Waals forces are primary drivers at the interface of biological and non-biological systems. Specifically how these layers are formed and how they behave at various distances is still not completely understood, but theories such as the DLVO theory are being developed in order to begin to explain what is happening.

11.2.ii Cell-Substrate Adhesion: Integrins

Integrins are transmembrane proteins that tether a cell to the basal membrane, also known as basement membrane, or basal lamina. Integrins are heterodimers of α and β subunits; integrin's α and β composition generates differences in both ligand specificity and strength of interaction. In mammals there are eighteen known α subunits and eight known β subunits which result in 144 potential difference combinations [20]. Integrin heterodimers adopt two possible conformation: a bent (closed) or upright (open) conformation [21]. Changes in physical conformation determines integrin activity; regulation of an integrin between an inactive (closed) or active (open) conformation regulates the binding affinity to ligands. Integrin based adhesion play key roles in cell signaling where the lack of integrin mediated cell-matrix interactions leads to cell death, and the defect of certain integrins can indicate a disease state. For example, defects in $\alpha 5\beta 1$ results in defects in blood vessel structure, somite formation, and neural crest migration; inappropriate $\alpha 5\beta 1$ can lead to severe skin blistering; defective $\alpha 5\beta 1$ is a trait of muscular dystrophy [18].

After initial binding events of integrins, adapter proteins are recruited in order to stabilize adhesion and create a meaningful adhesion point, often referred to as a focal adhesion complex (FAC). Adapter proteins, such as talin, are important for both stabilization and signaling, which locks integrins into the open (active) position and tethers the cytoplasmic tail of the intergrin β sub unit to

filamentous actin [22]. Talin is not exclusive in this job, and proteins such as kindlin can serve similar purposes [23] (Figure 2.4).

Integrin binding is a major component of mechanical signal transduction. There are two modes of mechanosensing in the cell via integrin binding. These are denoted as “outside-in” and “inside-out.” Outside-in denotes some external event acting as the mechanical stimulation; an example would be the elasticity of the substrate, which could act like a loose spring. When the cell binds to the ligand and establishes an initial FAC, several intracellular processes would determine if the cell creates a stable adhesion to that ligand, or continues ‘to look’ for others.

Inside-out is just the opposite, in which intracellular components control integrin binding. For example, integrins can be opened via adapter proteins, such as talin, thus increasing the affinity to bind to specific ligands. Because we are interested in viewing the cell as a tool to measure aspects of substrates, we will focus on this “outside-in” activation. Again, the primary difference is in the point of activation; that is to say whether the binding of some ECM protein opens the integrin, or an adapter protein such as talin activates the integrin from within the cell. After the integrin is bound to a ligand, there is a generally accepted series of steps that occur for the maturation of FAs.

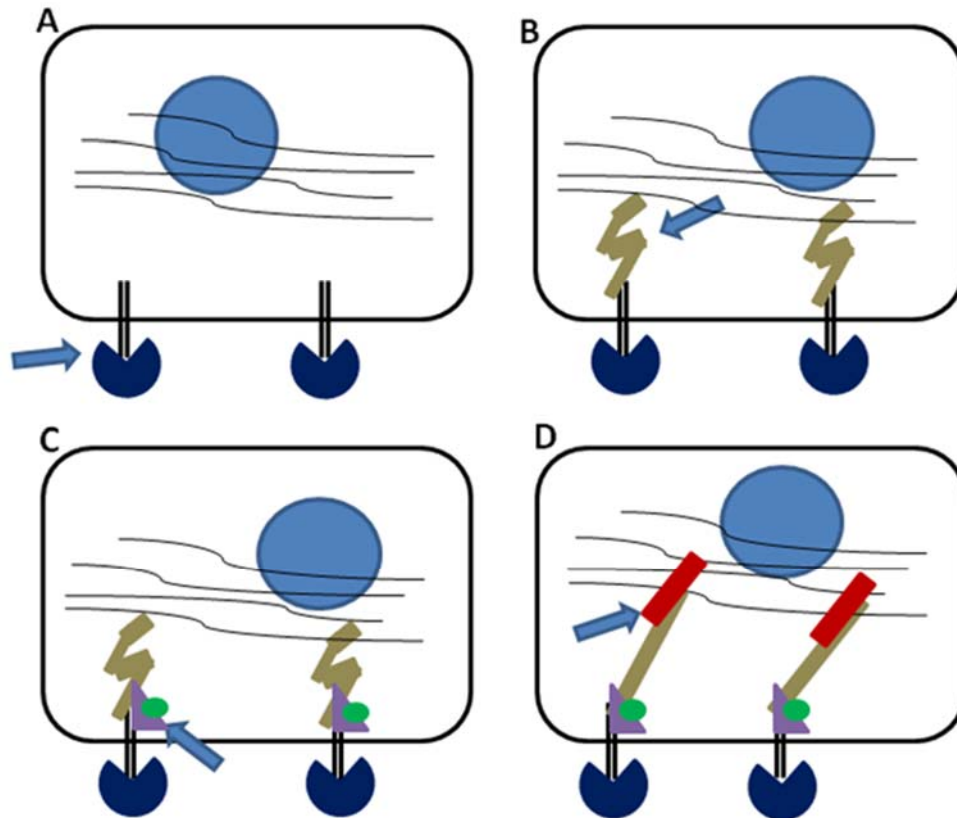


Figure 2.4. Overview of Initial Adhesion and FA Maturation.

(A) Integrins bind to ligands in the ECM. These proteins are often well-organized proteins in the ECM, such as laminin, fibronectin, and collagen. Such proteins help provide tissue organization or serve to reinforce function, such as the ECM in large muscle groups in the leg. (B) Adapter proteins such as talin and kindlin, marked by arrow, are recruited which stabilize the integrin and link it to the cytoskeleton. (C) Focal adhesion complexes are formed when other adapter proteins are recruited, such as paxillin and focal adhesion kinase marked with arrow; these proteins allow integrins to cluster and mature into a meaningful adhesion point. (D) Upon mechanical stress or some other signaling event, proteins such as vinculin are recruited, marked by arrow, that relay information from the ECM to the cell. In the case of vinculin, it is the mechanical force on the integrin, such as pulling, that opens adhesion motifs on talin where vinculin binds and reinforces the cytoskeleton link.

Talin is recruited to stabilize the integrin in the “open” conformation and link it to filamentous actin. It binds to the cytoplasmic beta-tails of integrins and links them

to the cytoskeleton. This integrin/talin/actin cytoskeleton interface serves as the assembly site of a large and complex intracellular signaling complex [21, 24, 25]. The adapter protein Paxillin and the kinase Focal Adhesion Kinase (FAK) cluster early in FAC development and participate in many signaling events related to adhesion [15, 26]. Later, other adapter proteins localize under specific conditions. The localization of Vinculin to FACs occurs in a force dependent manner [15]. Upon the application of force (i.e. pulling on the FAC), talin unfolds, exposing several binding sites for adapter proteins such as vinculin [15], though it should be noted that, as in the "inside-out" scenario, the recruitment of talin is not necessarily force dependent [27, 28]. Although these adaptor proteins are not the entire story in adhesion mediate signaling, they form a common piece of direct mechanotransduction. While the pieces of adhesion are beginning to be put together, the timing of each element is still not known, as well as how these dynamic forming FACs relate to Focal Adhesion Junctions (FAJ) in epithelial cell types [29].

Integrins play adhesive roles in another cellular junction, called hemidesmosomes; these junctions are an important cell-matrix adhesion molecule in an epithelium. These specific complexes anchor the epithelial layer to the basal lamina via laminin. They contain the specific integrin heterodimer combination $\alpha 6\beta 4$ and attach uniquely to keratin filaments via the intracellular proteins dystonin and plectin [18]. Hemidesmosomes contain several different molecules unique to this specific structure. Once thought to be primarily an

anchor for an epithelium, they are now understood to play a role in several signaling events much like the more mechanosensing integrin clusters of the $\beta 1$ group [30].

II.2.iii Cell-Cell Adhesion: Adherens Junctions

As described earlier, an epithelium is defined as a sheet or tube of cells that are bound to one another by cell-cell adhesion. These cell-cell adhesive interactions are essential for the stability and maintenance of an epithelium. As mentioned before, central to the cell-cell adhesion are the adhesion proteins called, cadherins. [31]. Cadherins are transmembrane proteins that bind in a homotypic, calcium dependent manner. The cadherin superfamily contains over 100 members that can be divided into four different groups: classical, unconventional, desmosomal, and protocadherin. In the canonical classical case, a cadherin protein in one cell binds with the cadherin of neighboring cell in a calcium dependent fashion; this enables the linking of the apical cortical actin cytoskeleton of these two cell and the formation of an adherens junctions (AJ). The linkage of the actin cytoskeleton to the AJ complex is mediated by the formation a α/β -catenin complex and the binding of this complex to the cytoplasmic tail of the cadherin [31].

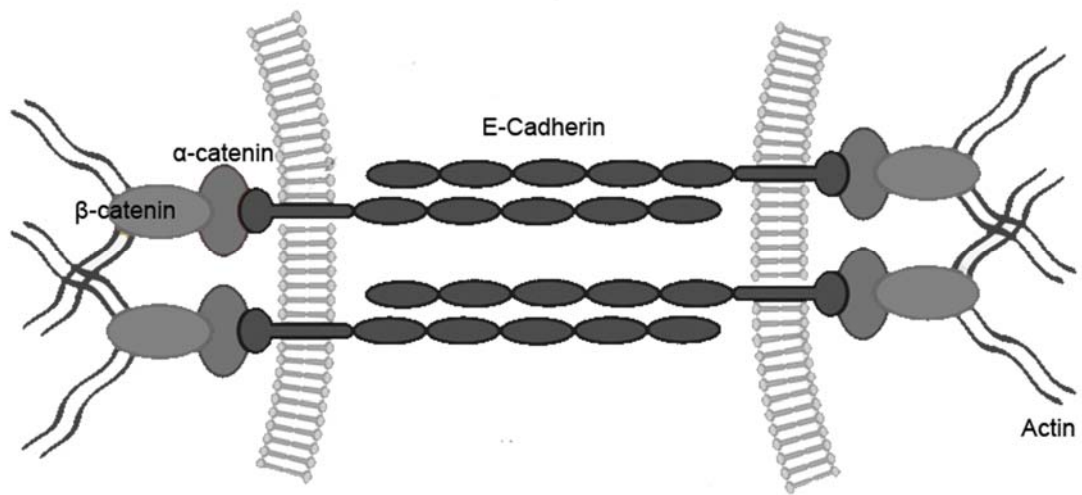


Figure 2.5. Overall Structure of the E-Cadherin Complex.

The intercellular domain binds with other e-cadherin proteins from neighboring cells. These binding events are dependent on Ca^{2+} ions. Once the proteins bind, creating a focal adhesion complex, linking it to a neighboring cell, α -catenin is recruited and stabilizes the cadherin complex.

How the catenin complex associates with the actin cytoskeleton is still not completely understood [32, 33]. However, it is clear that this complex along with the Rho family of proteins play a substantial role in the formation and regulation of AJs [34]. The tethering of cadherins to the apical cortical actin cytoskeleton creates an actin belt-like structure through the epithelium [18, 31]. This linkage forces the epithelial layer to act as a mechanical unit, which transmits force through the epithelium, or allows the movement of the epithelium as a common sheet during wound healing. These cells acting as a unit is one of the motivating features for this study, and the use of these types of cells. Without examining cell types with this specific cell-cell requirement one could not intelligently think about

what a substrate or device may do *in vivo*. For instance, one of the hallmarks of metastasizing cancer is the down regulation of e-cadherin [35], which can be coupled with cadherin switching where N-cadherin is up regulated at the same time [36, 37]. This allows cancer cells to break through barriers and invade. Another motivation is that e-cadherin plays an important role in development, and may be an avenue in which to control the fate of human embryonic stem cells (hESC). Expression of e-cadherin was been demonstrated as a possible treatment to increase the survival and self-renewal of hESC [38, 39]. Although this is not a universal feature for all stem cells. The expression of e-cadherin in somatic stem cells, or adult stem cells, is associated with differentiation [40-42]. In the case of either type of stem cell, the mechanisms underlying the differences in both situations are still not completely understood. E-cadherin can impact an overwhelming number of processes, those downstream of AJ and between membrane bound parts of the cell [43]. There is also a difference between the stability of e-cadherin complexes *in vivo* compared to *in vitro* assuring that there are many more discoveries awaiting researchers [44].

In recent years, the mechanical aspects of cells, both physical traits (such as elasticity) and physical manipulation (pushing and pulling), are understood to play an important role in cellular growth and behavior. The transmission of mechanical information through the epithelium has been shown to influence behaviors such as collective cell migration [45], or promote the invasive phenotype in cancer cells [46]. Organs are lined with an epithelial layer of cells

and these sheets of cells act as barriers, allowing passage of molecules that are needed and preventing those that may be harmful. Our bodies, and organs, are subjected to mechanical stress all the time, and it has been demonstrated that e-cadherin can tune the stiffness of cells proportionally to the applied force acting on them [47]. Also, the mechanical properties of these cells can be a sign of problems, as cellular stiffness is strongly correlated with the cancer cells ability to metastasize [48].

II.3 Adhesion On Engineered Substrates

It has been demonstrated that substrates patterned at the nanoscale exhibit interesting effects on cellular behavior. Below I discuss the role that nanoscale structure has been shown to affect protein adsorption and organization. Composition, organization, and mechanical properties of the ECM all play an important role in cellular behavior and growth.

II.3.i Protein Adsorption

Protein adsorption to a surface will significantly alter the intended effect of any specific application, such as implantable devices. Such devices must deal with immediate biofouling that occurs when introduced into the body. An understanding of how protein adsorption and organization is affected by various substrates is necessary in order to predict how cells and the ECM will interact with the surface. For example, titanium is a biocompatible material used for implants. The absorption of bovine serum albumin and fibronectin to rough and

smooth Ti alloy surfaces was examined using two methods: X-ray photoelectron spectroscopy (XPS), and radiolabeling. Cell attachment and proliferation were surface-roughness sensitive and increased as the roughness of Ti alloy increased. XPS and protein radiolabeling both showed that human serum albumin was adsorbed preferentially onto the smooth substratum. XPS technique showed that the rough substratum bound a higher amount of total protein (from culture medium supplied with 10% serum) and fibronectin (10-fold) than did the smooth one [49]. Surface topography may not represent the only structural organization that influences protein adsorption. Recent work demonstrates that high free-energy crystal facets tend to induce the arrangement of human plasma fibrinogen (HPF) as a thin globular protein layer [50]. These results suggest that lower free-surface energy grains locally shift the adsorption potential of a surface and lead to the formation of protein-protein networks; in contrast, nanofeatures impose physical limitations on the organization of proteins adsorbed onto surfaces; the free surface-energy being defined as the work required to increase the size of the surface of a phase. This can be quantified using techniques such as contact angle measurements with various fluids. In this case confining the diameters of observed ring-like protein networks [50]. Similar effects have been observed using nanoparticles, where the effects were similar to roughness or topography. Proteins adsorbed on smaller nanoparticles can retain their structure and function better than when adsorbed on larger nanoparticles [51]. Biologically compatible materials other than Titanium oxide have been used to study protein

adsorption. Aluminum oxide membranes with different nanotopographical features were prepared by anodic oxidation technique. Even though membranes with grains of 40 nm in diameter had a weaker ability of protein adsorption at the early stage, the final amount of adsorbed protein had no significant differences compared with other membranes. The study also noted that there was no real difference observed in mesenchymal stem cell (MSC) attachment between membranes [52].

Substrate roughness can also influence the organization and structure of proteins adsorbed onto surfaces. The elongated features of collagen adsorbed onto smooth substrata were no longer seen on rough substrata [16]. In order to investigate if surface chemistry could alter the effects seen with simple topographical changes, collagen was adsorbed onto smooth and rough substrates functionalized with CH₃ to achieve a hydrophobic surface and OH to achieve hydrophilic surface. A comparison of collagen adsorption on smooth and rough substrata functionalized with CH₃ (hydrophobic) and OH (hydrophilic) groups using alkanethiol self-assembly demonstrated greater amounts of protein on the hydrophobic surfaces. Therefore, while the amount of protein is primarily affected by surface chemistry (specific molecular composition of a material surface), the supramolecular organization of the adsorbed layer is controlled both by surface chemistry and topography [16].

Beyond surface structure, studies have investigated how hydrophobicity can affect various biological mechanisms. Hydrophobicity is a quantifiable

property of a surface measured by using the contact angle of various liquid drops residing on the surface [19]. The higher the contact angle (the more round the droplet) the more hydrophobic the surface is. And the opposite is true of hydrophilic surfaces, the lower the contact angle (the more spread out the droplet is) the more hydrophilic the surface is. In order to investigate how hydrophobicity affected protein adsorption (bovine serum albumin and fibrinogen), model chemistries of CH_3 (hydrophobic), and OH (hydrophilic) were used to functionalize surfaces. It was demonstrated that albumin undergoes adsorption via a single step whereas fibrinogen adsorption is a more complex, multistage process. Albumin was also shown to have a stronger affinity toward the hydrophobic surface compared to the hydrophilic surface. Fibrinogen adheres more rapidly to both surfaces, having a slightly higher affinity toward the hydrophobic surface. Conformational assessment of the adsorbed proteins by grazing angle infrared spectroscopy (GA-FTIR) shows that after initial 1 h incubation, few further time-dependent changes were observed [53].

Cellular interaction with a surface is often thought of as cells interacting with the adsorbed proteins on the surface and not the actual surface itself [11]. Therefore, using self-assembled monolayers of alkanethiols, which provide a flat and chemically well-defined surface, adhesion of human umbilical vein endothelial cells (HeLa) was examined. It was shown that cellular adhesion was primarily affected by wettability with surface functional group, its density, and cell type playing a lesser role [54]. This, along with other data, suggests that protein

adsorption may only influence the cellular response to nanotopography during initial cell-substrate contact [55].

II.3.ii Nanoscale Influences on Cellular Behavior

Recently, many different patterned surfaces have been tested to determine how cells would react to them; this work has begun to illuminate the responses of cells to micro and nanopatterned substrates [56]. It is well known that aligned microscale grooves patterned into a substrate will affect cellular behavior [11, 57]. Similar nanoscale patterns on substrates also affect cellular behavior and these results demonstrate the potential that topographical manipulation may hold for controlling and regulating cellular behavior and response. For example, human Mesenchymal Stem Cells (hMSCs) cultured on 350 nm gratings of tissue culture polystyrene (TCPS) and PDMS have decreased expression of integrin subunits $\alpha 2$, $\alpha 6$, αV , $\beta 2$, $\beta 3$, and $\beta 4$ compared to the unpatterned controls. Also, hMSCs elongated on the gratings exhibiting an aligned actin cytoskeleton while unpatterned substrates showed cells spreading with random but denser actin cytoskeleton network [58]. Varying groove width changed the orientation and maturation of focal adhesions [10]. Grooves patterned between 100 nm to 1000 nm aligned more than 50% of cells cultured on such substrates [59]. C/EBP δ , a tumor suppressor transcription factor that induces gene expression involved in suppressing cell migration, when ablated, decreased cell size, adhesion, and cytoskeleton spreading on 240 nm and 540

nm grooves [60]. Nanogrooves of 100-300 nm grooved ridges and 100-300 nm pillar diameter gaps were found to enhance focal adhesion complex development effectively, which enhanced human neural stem cells differentiation toward neurons and astrocytes [13].

Nanofibers have also been shown to influence cellular behavior. Human tendon stem/progenitor cells (hTSPCs) were cultured on nanofibers. hTSPCs were spindle-shaped and well orientated on the aligned nanofibers compared to random oriented fibers. Expression of tendon-specific genes were significantly higher on aligned nanofibers compared to random oriented fibers, both in normal and osteogenic media. In contrast, randomly oriented fibers induced osteogenesis. Also, aligned fibers expressed higher levels of integrin $\alpha 1$, $\alpha 5$, and $\beta 1$ subunits and myosin II B [61].

The cellular response to nanopillars are slightly different than nanogrooves because they do not form channels but rather sharp, high curvature points for cellular contact. Simple changes in topographical organization using nano-pillars was used to demonstrate how cellular adhesion is influenced by nanotopography. In this study, nanopillars were produced by polymer demixing (polystyrene and poly(4-bromostyrene)) with sizes 13, 35, and 95 nm. Endothelial cells showed greatest response on 13 nm pillars with increased spreading and well-defined cytoskeleton [62]. Substrates patterned with 14 nm disordered features showed greater cytoskeleton organization, adhesion, and increased expression of Runx2, osteopontin, and osteocalcin compared to planar

controls [63]. In another study, fibroblasts and endothelial cells were co-cultured on a substrate patterned with nanopillars with height continuously changing from planar to 250 nm over a total distance of 9 mm. It was shown that cells were selective with fibroblasts preferring smaller features and endothelial cells preferring larger features near 75 nm. It was concluded that 75 nm features provided smallest fibroblastic adhesion [64]. Another study concluded reduced fibroblastic adhesion on nanopillars created by polymer demixing at size 50 nm [65]. Also, rat calvaria bone cells were cultured on 35 and 95 nm random nanopillars. Initial adhesion favored the smaller nanofeatures but the effect diminished over time with cells showing no difference [66]. In yet another study, 160 nm high nanocolumns were produced using colloidal lithography. Fibroblasts were shown to have fewer mature focal adhesion complexes compared to planar controls [67]. Also, nylon tubes with internal nanotopography created by polymer demixing influenced fibroblast adhesion, spreading, morphology and cytoskeletal organization. It was noted that tube diameter did not affect cells [68]. A 1718 gene microarray performed on cells cultured on nanocolumns identified several genes that are regulated by topography [69], as well as cells demonstrating an altered nuclear organization [70]. The expression of genes essential for osteogenesis and cell adhesion was significantly decreased on nanopits, but up-regulated on nanoislands/nanopillars [71]. Considering all of these data, no clear fundamental rules have emerged to explain all phenomena in a general sense. It seems that each size variations produced slightly different effects on adhesion,

but it is not clear how cells read the surface and preferentially bind to one size over another. However, there are trends that can be seen between distinct geometries. Pillars have not been shown to polarize cells as grooves have been. To fully take advantage of nanopillars, further studies are needed to understand how the cell fundamentally react to this feature type.

As discussed with protein adsorption, the nanoroughness of a surface can vary interactions of cells, and proteins with surfaces. Instead of looking at specific proteins, these studies investigated interactions at the cellular level. For example, endothelial and osteoblast cells were cultured on features less than 100 nm and greater than 100 nm. While the surfaces with features greater than 100 nm had the greatest surface energy and cell densities, surfaces with features less than 100 nm were more efficient with greater change in surface energy and cell density with respect to smallest change in surface area and roughness [72]. Increased surface roughness was achieved by electrospun fibers with nanobeads. Roughness was shown to increase adhesion, spreading, and osteogenic differentiation of rBMSCs [73]. Rat bone marrow-derived mesenchymal stem cells (rBMSCs), human BMSCs (hBMSCs) and primary human adipose-derived stem cells (hASCs) were studied on 12 mm substrate patterned with pore sizes of 2 μm down to a few nm. All cell spreading was decreased on surfaces with increased pore size. Attachment density was cell type dependent with rBMSCs and hBMSCs having lower densities on porous gradient compared to planar controls, and hASCs showed a peak density on

pore size region of 329 ± 129 nm. It was noted that rBMSCs were more sensitive to the pore size change compared to hBMSCs. This study and a similar work demonstrated that nanostructured Ti surfaces show increased adhesion, proliferation, and osteogenic differentiation of MSCs [74, 75]. Nothing that surfaces with random nanofeatures can influence cells, *Zeiger et. al.* [76] explored polystyrene tissue cultures dishes and found different topographical features from brand to brand. This could suggest that the anecdote of certain tissue culture dish brands as being more favorable for certain cell types may have some validity [76].

II.4 Probing the Mechanical Properties of Cells

The mechanical aspect of cells have recently gained attention with the development of new tools and an understanding of correlations between the elastic properties of cells and various behaviors [77]. Below I review some information regarding the characterization of materials needed to consider the mechanical properties of cells. I also discuss Atomic Force Microscopy, both fundamental information regarding the technique and a specific acoustic measurement method used in this study. This will provide the tools and background necessary to consider the data collected in this work.

II.4.i Cells as Viscoelastic Materials

Different materials deform differently under stress. How the material reacts under stress is a major property of that material. Some materials deform only a

small amount and return to their original state. Others deform some amount but never return to their original state. Other materials, such as liquids, have no real solid configuration, taking the shape of whatever container they are in and produce effects such as drag. Materials that deform and then return to their original state are considered to be elastic (Figure 2.6). Within the linear regime, that is one that can be modeled as an ideal spring, the constant of proportionality between the stress and strain is called the Young's Modulus.

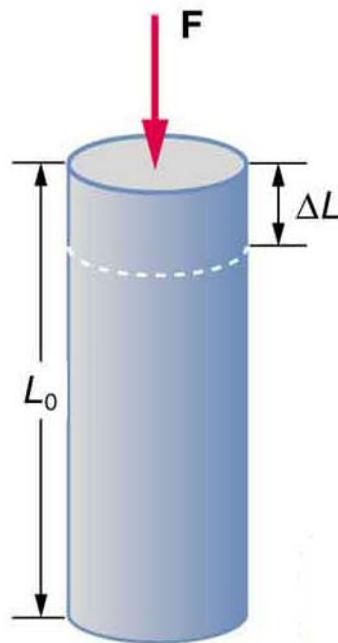


Figure 2.6. Stress and Strain.

Stress is defined as the intensity of force (F) at a point, as $\sigma = \Delta F / \Delta A$, as $\Delta A \rightarrow 0$, where A is the area over which the force is applied. Strain is defined as $\epsilon = \Delta L / L$, where L_0 is the initial length and ΔL is the change in the length due to the strain.

Likewise, a liquid is considered to be viscous if it produces some drag. This is not a simple linear relationship, but is dependent upon the velocity of the mass moving through the particular liquid of interest, and also such properties as compressibility. Elastic materials can often be modeled as a resistor and viscous materials modeled as a dashpot. Other materials, such as plastics, have a combination of elastic and viscous properties. These materials are considered to be viscoelastic materials. Biological systems are examples of viscoelastic materials [78]. As such, when force is applied to cell membrane there is a strain and after some time the cell membrane will return to something close to its original state. The cell membrane is fluid however, made up of phospholipids, lipid rafts, and various transmembrane proteins, and as such there will be both elastic properties and viscous properties. Therefore, the resistance to stress will be dependent on how fast the stress is applied and there could be a significant time lag before the membrane returns to the initial form. Viscoelastic materials can be modeled as a resistor and dashpot in series.

II.4.ii Basics of Atomic Force Microscopy

Atomic Force Microscopy (AFM) is an analytical technique used to image things at an atomic resolution using a very sharp point on a cantilever that bends according to the properties of both the cantilever and the sample being imaged; The basic setup of an AFM is relatively simple; there is a cantilever with a sharp tip that is brought either close to or in actual contact with the sample. There are

three basic modes of operation for a standard AFM: tapping mode (or intermittent contact mode) which oscillates the cantilever so that the tip taps the substrate with a relatively high frequency, contact mode, in which the tip moved across the sample, and non-contact mode, in which the tip is oscillated just above the sample but never contacts the sample (Figure 2.7).

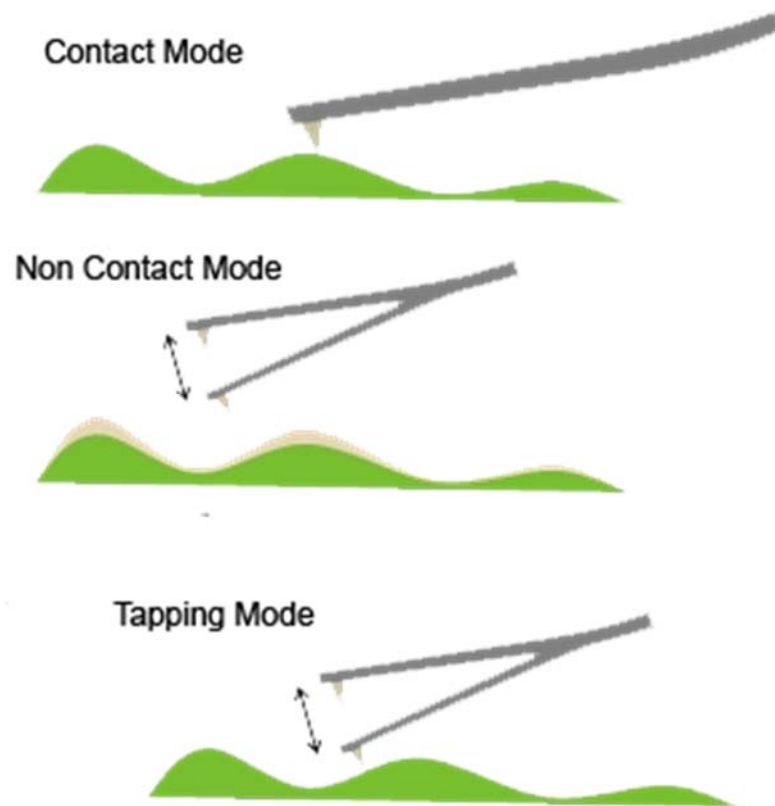


Figure 2.7. Modes of Operation in the AFM.

Contact mode drags the cantilever across the substrate. A set point is determined before imaging, deviation from this set point is input into the feedback loop that adjust the height of the piezo to maintain the given set point thereby mapping the topography of the sample. Non-contact mode oscillates the tip and measure a phase shift in the to determine that some interaction has occurred. Tapping mode (Intermittent contact mode) physically interactions with the surface, where a shift in phase and the deflection are measure and input into the feedback loop so that a high-resolution image of topography is attained.

Tapping mode is a common method of imaging; it allows high-resolution images with only a small chance of damaging the tip. The largest limitation in this mode of operation is noise, which can be difficult to eliminate. This noise is generally related to the aspect ratio of your sample. Very high aspect ratios

required gains to be set high in order for the tip to respond in enough time to provide a proper image, but higher gains can mean increased noise. Contact mode can also provide high-resolution images. One of the main advantages of contact mode is the ease in which samples can be imaged in liquid. Because the tip is in contact with the sample, the risk of contact mode is that tip inevitably wears and imaging quality will be reduced due to damage. Non-contact mode has the advantage of never actually being in contact with the sample, which means the tip will likely last for a very long time, however, the forces imaged in this mode can easily be skewed due to different external conditions. These are often very small and can result in a low signal to noise ratio.

A laser reflected off of the cantilever onto a photodiode measures tip deflection (Figure 2.8). A photodiode is used in order to achieve the high resolution seen in AFM. Briefly, a laser spot is focused onto the center of the photodiode, which returns the sum voltage of all four quadrants. Deflection is given as the difference of the sum of the top two and bottom two quadrants. Friction, which is the twisting action of the cantilever, is measured as the difference of the sum of left two and right two quadrants. In this manner, motion in all three degrees of freedom can be measured.

Atomic Force Microscope

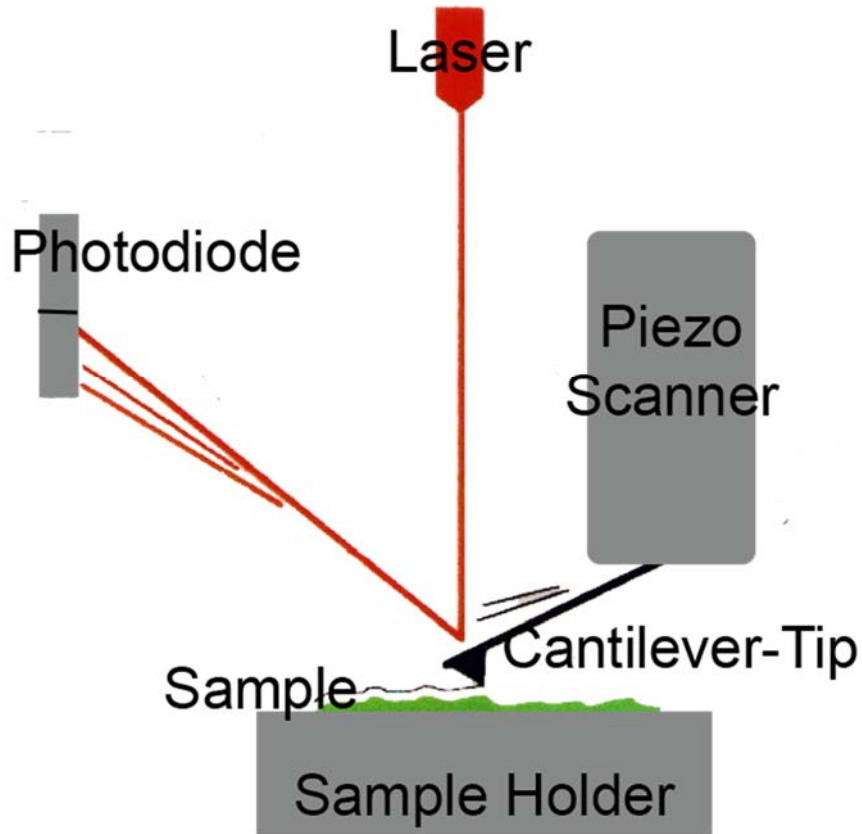


Figure 2.8. Simple AFM Setup.

A laser is reflected off of a cantilever onto photodiode. Motion is measured as the difference of the top and bottom or left and right halves. The cylindrical piezo scanner depicted here is not the only mode of operation. The sample holder itself is sometimes the mechanism by which the sample is moved.

The quality of an AFM image can depend on equipment as well as sample prep.

A piezo is often used to control the motion of the cantilever. If this material is not maintained properly data can be obscured due to the lack of responsiveness. For example, after imaging in one direction, the return raster scan should produce the same image. If this is not the case, it could point to a damaged piezo head. A

broken tip can produce a doubling effect, where every feature has a shadow of itself. A rounded tip will show features that are larger than they actually are, as the tip sharpness will determine the resolution of the image. Thermal conditions can affect the oscillation of the cantilever producing artifacts in the image. Low gains, a scan speed that is too high, or a non-responsive piezo can produce a smearing effect, where images appear to be blurry. The spring constant of the cantilever can also lead to a smear effect if the sample being imaged has a smaller Young's (or dynamic) modulus than the cantilever.

In order to effectively use the AFM, an appropriate probe must be chosen for the intended sample. High aspect ratio features require a pillar shaped probe in order to physically fit in between surface features. Otherwise, a true representation of the surface is not attained, measurements are skewed by tip geometry. It would be impossible to distinguish between deflection due to the side of the probe and deflection due to the tip of the probe interacting with the sample. Likewise, when measuring the elasticity of samples, probes with an appropriate spring constant is required. A spring constant that is too stiff will hide variations in mechanical properties, the surface will not be stiff enough to bend the cantilever. If the spring constant of the cantilever is too small then the image will only show the deflection of the cantilever without any surface information. The probe will not be able to deform the sample. Beyond the physical shape or mechanical properties of the cantilever, it is often advantageous to have a specific material composition. For example, the surface charge on SiO_2 is more

negative than SiN₄. The former could potentially be more reactive with respect to medium components, such as proteins in fetal bovine serum, compared to the later.

II.4.iii Force Modulation Microscopy for Studying Biological Samples

The AFM allows investigators to map the mechanical properties and adhesion forces of thin films in aqueous solutions with nano scale resolution. AFM has a broad range of applications in the material and biological sciences [79-98]. However, cantilever dynamics are difficult to understand and data difficult to interpret. This can lead to conflicting results [99, 100] and has limited the use of promising methods of imaging with AFM, such as Force Modulation Microscopy (FMM) [101]. Nevertheless, FMM is a potentially powerful acoustic method for mapping surface mechanical properties in fluids. Typically, the probe is kept in contact with the sample, such as in contact mode, and an additional oscillation is added in the z direction. This combines contact mode with the principles of tapping mode and allows high contrast imaging of soft samples, which are not otherwise easily obtained.

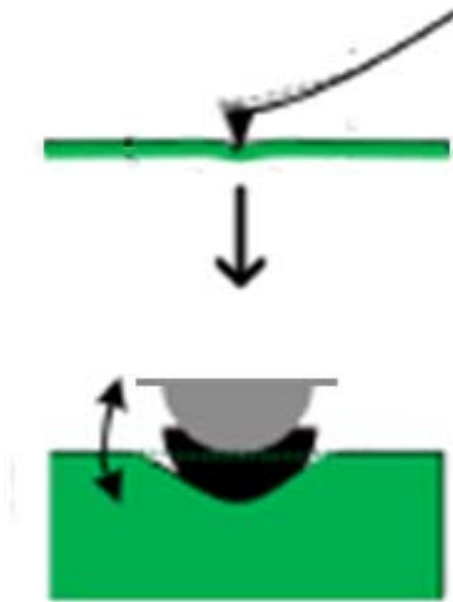


Figure 2.9. Force Modulation Microscopy with the AFM.

As in contact mode, the tip is in constant contact with the sample (top image). As noted below, this applied force has an optimal range in order to reduce nonlinear effects of cantilever dynamics. As the tip is in contact with the sample (bottom image), a z directional oscillation is applied, allowing elastic measurements with high lateral resolution.

Quantitative analysis of data obtained can be difficult to understand, as noted above. There exists a viscoelastic model of surfaces in air [102-104] but no such analogous model exists in fluids. Hertzian contact theory can be used as a first approximation in modeling contact mechanics such as found in FMM. However, there are a few limitations in using Hertzian contact theory, as the model assumes a non-adhesive and elastic contact between a rigid spherical tip and substrate, and is most useful when the static contact force is much greater than the adhesion force [105-107]. An extension of the Hertzian model, which includes

adhesive forces, can be found in such models as Derjaguin-Muller-Toporov (DMT) or Johnson-Kendall-Roberts (JKR) [108], allowing for greater utility overall.

For simplicity, the Hertzian model has been the model of choice when analyzing mechanical properties with the AFM. For lossless contact and certain modulation frequencies, the cantilever can be modeled as two springs in series, which gives the cantilever deflection as [109]:

$$u_c = \frac{z_0 k^*}{k_c + k^*} \sin \omega t$$

where z_0 is the amplitude of contact, ω is the angular frequency of oscillation, k_c is the spring constant of the cantilever, and k^* is the contact stiffness:

$$k^* = \sqrt[3]{6FRE^{*2}}$$

where E^* is the reduced Young's modulus, R is the tip radius, and F the applied force. This simplification provides an explanation for FMM amplitude images where cantilever dynamics, as would be encountered in an aqueous environment, are not present. In order to probe the properties of biological materials it is important to have the tools to investigate these materials in physiological conditions. This requires something more than the simple linearized model above. Hence, one can model cantilever deflection with a second-order harmonic as [109]:

$$u_c = \frac{k_c^2 z_0^2 \beta}{4(k^* + k_c)^3} + \frac{z_0 k^*}{k^* + k_c} \sin \omega t - \frac{k_c^2 z_0^2 \beta}{4(k^* + k_c)^3} \cos 2\omega t$$

where β is:

$$\beta = \frac{\partial^2 F}{\partial h^2} = \sqrt[3]{\frac{4R^2 E^{*4}}{3F}}$$

This is called the second-harmonic factor. One can derive this expression by taking the Taylor series expansion about the tip indentation. This formulation provides an opportunity to consider higher order cantilever dynamics. It is worth noting that the zeroth order term in this formulation reflects a DC deflection, and as such demonstrates that the task of clearly deconvoluting the topographically induced deflection from a desired FMM response is difficult to say the least [110]. However, the first and second order terms do not affect the feedback loop and can be detected by lock-in techniques [101]. *Zhang, et. al.* [109] concludes a few points in an effort to build a quantifiable model for FMM images: changes in surface elasticity can lead to nonlinear effects in FMM, hence the need to expand on previous linearized Hertzian models; the first harmonic can be related to the elasticity of the substrate, while the second harmonic is a measure of the nonlinearity of the cantilever in contact, which means that in order to accurately interpret data in FMM images the ratio of the second harmonic to first harmonic should be less than 1%; in order to have a complete working model in which FMM can be used and interpreted reliably for soft polymeric and bimolecular thin

films, a viscoelastic model must be included [109]. It is clear that there is much work that needs to be done before FMM can be fully utilized. Presented here is a good starting point to work from in order to begin to take advantage of FMM for studying live, dynamic biological samples, or soft complex polymeric thin films.

11.5 Summary

In this thesis I considered a model epithelium and how it interacts with various substrates. Above, I have provided the background, framework, and context for this work. Since a model epithelial cell type was used I considered the principle parts of an epithelium in order to understand the behavioral implications of results. I was interested in how cells interacted with substrates, and therefore principle adhesion mechanisms were also reviewed, namely integrins and adherens junctions. Integrins mediate cell-matrix adhesion is central to the cells interaction with underlying substrate by regulating many important cellular pathways. Adherens junctions are a hallmark of an epithelium. They also take part in many signaling events related to cellular behavior and can play a part in compensating for adhesion situations considered in the work. Because of the interest in the biotic-abiotic interface, I reviewed the interactions of proteins with nanostructured materials as well as presented several examples of work that has been done with materials intended to influence cellular behavior through some structural property at the nanoscale. Such a consideration affords a context in which this work fits and gives an overall sense of how the data here could be

used. Finally, I covered the AFM as a means to probe the mechanical properties of cells on substrates of interest using FMM. To provide background information required to interpret data presented in this work, operation and techniques were covered, as well as limitations. In this work I set out to accomplish three primary goals: to determine the limit that topographical changes affect cellular behavior, define the responses of cells to these changes and identify the mechanisms that cells use to read the variations in such substrates. Additionally, I characterize the mechanical differences of the cells on the substrates and develop techniques to study mechanical properties of cells.

CHAPTER III

INVESTIGATING THE LOWER LIMITS OF THE EFFECT OF NANOTOPOGRAPHY

III.1 Introduction

Nanotopography influences many aspects of cellular behavior such as morphology and shape, differentiation, and growth. Mechanotransduction is the primary mechanism by which topography influences cells [11, 24] and complicates the understanding of the role nanotopography in cellular growth and differentiation. The physical properties of the extracellular matrix play an important role in regulating many cellular processes. The fact that cells respond to physical cues in their microenvironment has been known for quite some time, as the term contact guidance was first used in the mid-20th century [69]. Recently with the advent of new and sophisticated fabrication techniques, scientists have moved from the microscale to the nanoscale and found that cells respond to nano-patterned substrates in profound ways. Nanotopography has been shown to affect cell adhesion both positively and negatively [11]. Fibroblasts cultured on 27 nm features created by polymer demixing exhibit increased initial adhesion [111]. Cell based adhesion is dependent on the size and distribution of surface topography; small 20 nm nano-islands of structure increased cell adhesion in both fibroblasts and mesenchymal stem cells, but interestingly an increased in size of the structural islands, cells

became less adhesive[112]. Nanogrooves and nano scale fibers align cells [11, 113], which in the case of myocytes increases myogenesis [11, 114, 115]. In contrast, randomly oriented nanoscale features facilitates cell spreading [11, 73] which in the case of osteocytes accelerates osteogenesis [11, 63]. Organized pits can limit adhesion and up regulate adipogenesis [11, 116]. It has been show that a cell can detect a nanoscale features down to 10 nm [117].

The question still remains: what is the minimal nanoscale feature that cells respond on a nanostructure structured surface? This is important when designing a microscale or nanoscale biologically interfacing device, because nothing is known regarding the effects of nanoscale variation in the sub 10 nm realm on cell growth. To investigate the minimum feature size of a surface that influences cellular behavior, we used Madin-Darby canine kidney (MDCK) cells and NIH3T3 fibroblasts cultured on glass cover slips and 5x5 mm Si Wafers. It is well known that tissue culture cells grow on glass and in this paper we show that standard glass coverslip that are often used in tissue culture experiment have an inherently nanostructured surface with random features in the sub 10 nm range, making it an ideal control to determine the role that sub 10 nm structures affect cellular behavior. By culturing cells on a virtually atomically flat Silicon Wafer, we demonstrate a differential growth and morphological responses to sub 10 nm nanostructures that is associated with cell density and cell type.

III.2 Materials and Methods

Substrate Preparation: Si Wafer were purchased from Ted Pella, Inc., product #16008; wafer was precut into 5x5 micro-meter bits. Glass substrates were Fisher Brand Microscope Cover Glass (1 oz.), 22x22 mm, 12-542-13, LOT# 050610-9. Substrates were cleaned by 10 min. wash in Acetone at 70° C, followed by 2 min. wash in methanol, then substrates were cleaned with RCA-1 cleaning procedure: 1:1:5 of ammonium hydroxide, hydrogen peroxide, deionized water.

Cell Culture: MDCK epithelial cells and NIH3T3 cells were used. MDCK cells were cultured with HyClone DMEM/High Glucose cell media, cat#: SH30022.01, 4.00 uM L Glutamine, 4500 mg/L Glucose. NIH3T3 cells were cultured with [DMEM]. In each experiment, which was repeated at least three times, cells were cultured in a small petri dish and placed in an incubator at 37.6° C at 6% CO₂. Experiments were run at 30 minutes, 2 hours, 4 hours, 1 day, and 4 days. Cells were seeded at a concentration of 2.5×10^4 cells/ml (low concentration) and 6.4×10^6 cells/ml (high concentration).

Cell imaging: Cells were fixed with 4% Paraformaldehyde, Sigma-Aldrich (P6148-1KG), stained with Hoechst 33342 at 1:3000 dilution, Phalloidin 488 at 1:1000 in 1XPBS. Imaging was done with Zeiss Observer.21 Confocal Microscope, Axio Rel. 4.8 software. Cells were mounted with Aqua Poly/Mount, Polysciences, Inc. cat#: 18606. For cell viability and island growth experiments, we examined cell viability using an Acridine Orange/Ethidium Bromide procedure. We imaged the

all samples using a Zeiss Axio Observer Z1, Spinning Disc Confocal Microscope. Significance was measured using the student ttest. P values less than 0.05 were considered significant; parameters were selected as one tail, unpaired.

AFM measurements of Substrate surface topography: Substrates were cleaned by standard RCA-1 protocol, placed in a cleaned Petri dishes, and sealed with Para film inside level 7 cleanroom conditions prior to each experiment. For each experiment, the sealed Petri dishes were opened and placed immediately in the AFM to minimize the amount of organic contaminant during AFM imaging.

III.3 Results

We investigated the limits of the size of nanoscale structures that influence cellular behavior by culturing cells on a glass cover slip and Si Wafer. We chose glass because of inherent sub 10 nm features on the surface, whereas the Si Wafer is nearly atomically flat. The glass cover slip is amorphous silicon, with small, irregular nanostructures on the surface that are on average 5-10 nm in height (Figure 3.1A). In contrast, the Si Wafer is crystalline silicon with a virtually nanostructure free, “nanosmooth” surface (Figure 3.1B). We used these two substrates to investigate the role of surface nanostructure on cell growth and cellular morphology independent of surface chemistry, as glass and the Si Wafer share identical surface chemistries. Both surfaces, especially the Si Wafer were thoroughly cleaned prior to all experiments.

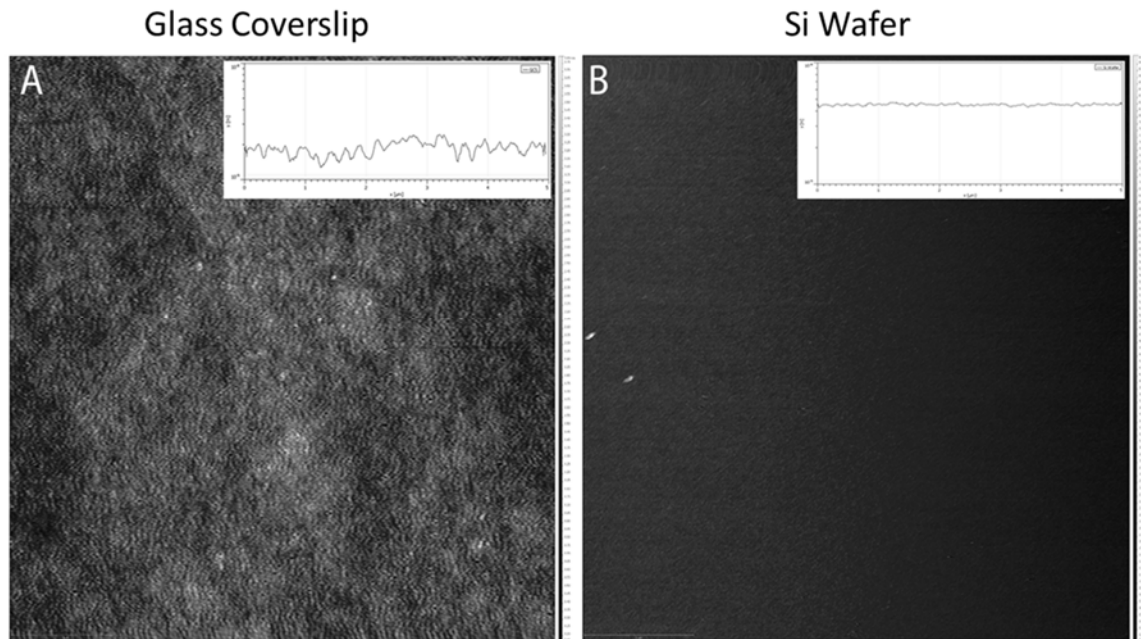


Figure 3.1. AFM Images of the Topography of the Glass and Si Wafer Substrate Used in this Study.

(A) AFM of Glass coverslip, inset a graphical representation of the surface; (B) Si Wafer with image size 5x5 μm , inset a graphical representation of the surface. Profiles are filtered, log scale in order to show an easily understood sense of the topographical differences. Nano features were measured at $<5 \text{ nm}$ on glass cover slips. There was slight tip drift in x directions for (B) which did not affect results, profile was in principle the same in both x and y directions.

If not cleaned properly (see methods), the Si Wafer demonstrated interesting effects on cellular growth and morphology. Specifically, the nuclei as shown by Hoechst staining were qualitatively larger when compared to glass controls. We suspect this is due to the presence of contaminants such as metal oxides on the wafer that are not removed with a simpler cleaning procedure like an acetone wash.

To determine whether cell density has any effect on the growth of cell on “nanorough” (glass) or “nanosmooth” (Si Wafer) surfaces we cultured both

MDCK cells and NIH3T3 cells at low (2.5×10^4 cells/ml) and high densities (6.4×10^6 cells/ml) on our substrates. While NIH3T3 cells at either density showed qualitatively less of a difference in growth on either substrate than MDCK cells (Figure 3.2 A,B,E,F), MDCK epithelial cells cultured at lower concentrations showed a qualitatively greater difference in growth when grown on Si Wafer as compared to Glass (Figure 3.2 C,D,G,H). MDCK cells exhibited growth to confluence on the glass substrate when compared to the Si Wafer at the low cell concentration concentrations (Figure 3.2C, Day 1; 3.2G, Day4). We observed that typically on the glass substrate MDCK cells plated at the lower concentration flattened and spread on contact with the substrate and begin to divide, initially forming isolated islands of cells (Figure 3.2C); by Day 4 the cells will form a nearly confluent epithelial monolayer (Figure 3.2G). MDCK cells plated onto the Si Wafer at lower concentration deviate from this normal growth: at Day 1, MDCK cells on the Si Wafer form small islands that are comprised of few cells furthermore these islands are rounded and lack a spreading morphology (Figure 3.2D); after four days of culture on the Si Wafer, the small rounded islands of MDCK cells remain as on Day 1 except fewer in number (Figure 3.2H).

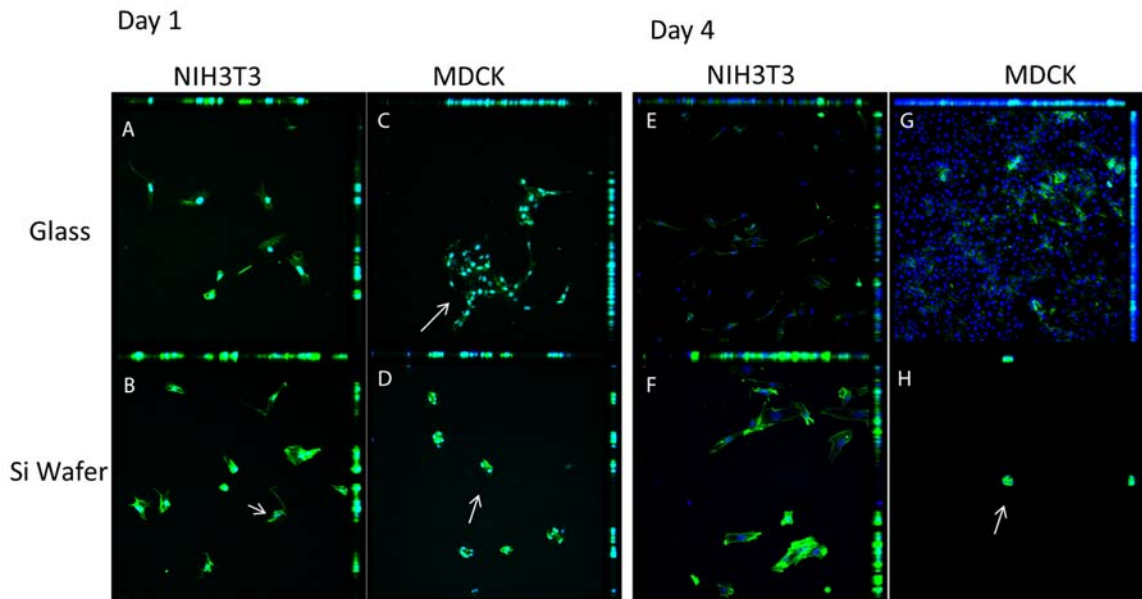


Figure 3.2. Growth of MDCK and NIN3T3 Cells on Glass and Si Wafer with “Low” Concentration of Cells.

(A) Glass Cover Slip, NIH3T3 cells at 1 day. (B) Si Wafer substrate, NIH3T3 cells at 1 day, note spreading of cells; (C) Glass Cover Slip MDCK cells at 1 day, cells are clustered on substrate in small islands (arrow), (D) Si Wafer MDCK Cells at 1 day, cells are isolated and found in small round clusters of 3-4 cells (arrow); (E) Glass Cover Slip, NIH3T3 cells at 4 days; (F) Si Wafer, NIH3T3 cells at 4 days (G) Glass Cover Slip, MDCK cells at 4 days, cells are confluent and cover the entire surface; (H) Si Wafer, MDCK cells at 4 days, cells remain in small round cluster, fewer in number than day 1 (arrow). Cells were counted on day 1 and compared to day 4. 10x Objective, 5 μ m field of view.

When cultured at a higher initial concentration the cells (6.4×10^6), the MDCK cells behaved differently with regard to growth but not morphology (Figure 3.2). The growth of cells (both NIH3T3 and MDCK cells) showed no significant difference ($p > 0.05$) when grown on either glass or the Si Wafer, as determined by counting nuclei stained by hoescht.

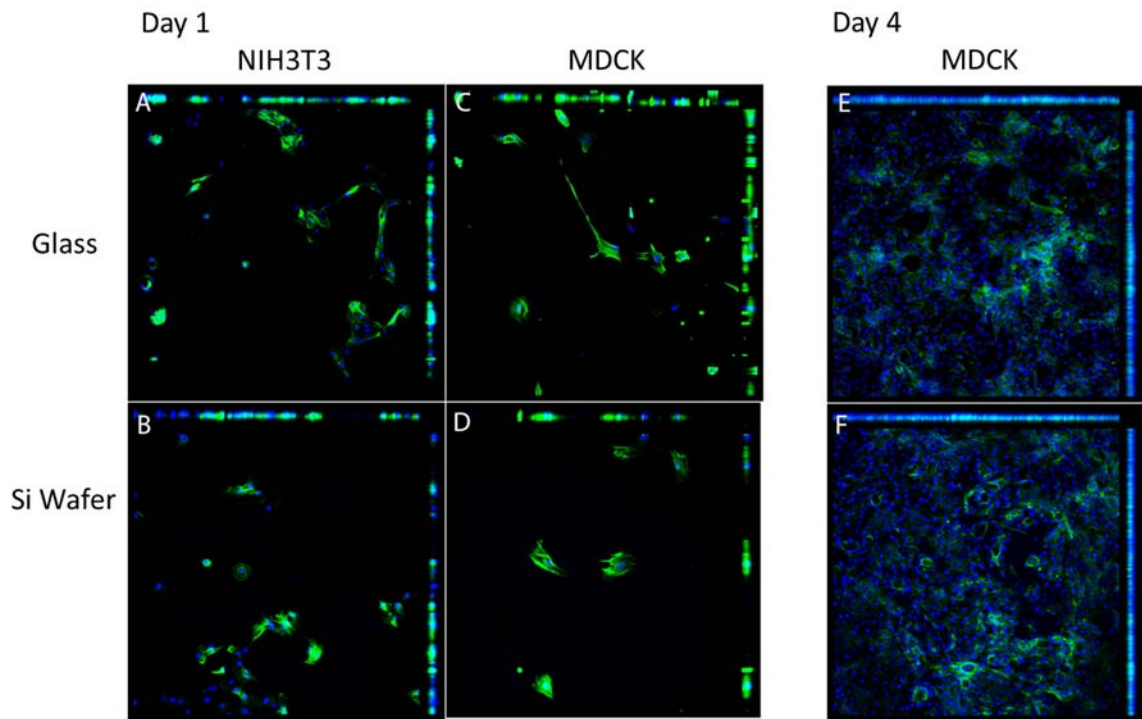


Figure 3.3. Growth of MDCK and NIH3T3 Cells on Glass and Si Wafer with “High” Concentration of Cells. (A) Glass Cover Slip, NIH3T3 cells at 1 day. (B) Si Wafer substrate, NIH3T3 cells at 1 day, note spreading/extension of cells; (C) Glass Cover Slip MDCK cells at 1 day, cells are clustered on substrate in small islands (arrow), (D) Si Wafer MDCK Cells at 1 day, cells are isolated and found in small round clusters of 3-4 cells; (E,F) Glass Cover Slip, MDCK cells at 4 days, cells are confluent and cover the entire surface; 10x Objective, 5mm field of view.

In addition to altered growth, MDCK cells exhibited an altered cellular morphology as well. This was evident by less spreading and a more rounded appearance of the MDCK cells on Si Wafer when compared to glass controls (Figure 3.4, compared A to B). When plated at a low starting concentration MDCK cells initiated growth in small clusters or islands of cells rather than as isolated, single cells.

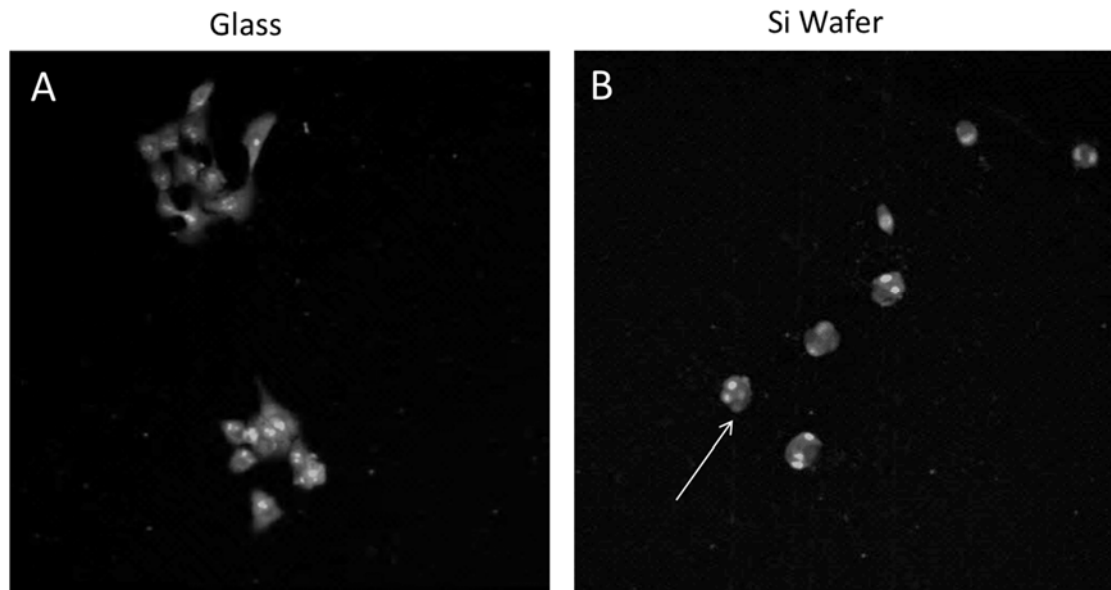


Figure 3.4. Preferential “Island” Growth of Epithelial Cells. (A) Glass Cover Slip, MDCK Cells show more cells per island than those grown on Si Wafer substrate and have a more spread morphology. (B) After one day of growth on Si Wafer, MDCK cells have formed small islands, with a rounded morphology (arrow). 10x Objective, 5 mm field of view.

While both substrate demonstrated similar number of cells at day 1, determined by counting nuclei using heochst, after four days of growth those on the glass substrate grew to near confluence while those MDCK cells on the Si Wafer substrate were lost resulting in qualitatively few cells present (Figure 3.2H).

While the frequency of MDCK islands per field of view was the same on both the Glass and Si wafer substrates, the number of cells in each island varied greatly.

Table 3.1. Island Organization at a Low Starting Concentration of Cells.

Substrate	Glass Cover Slip		Si Wafer	
	Day 1	Day 4	Day 1	Day 4
Average number of Islands per field	3±1 (n=8 fov)	NA, Confluent	3.55±1.5(n=9 fov)	NA, no islands
Average number of cells per Island	8.6±9.2cells/island (n=21)	NA. near confluent (see Figure 3.2G)	3.74±1.5 cells/island** (n=29)	NA, no islands (see Figure 3.2H)

**P=0.025, fov – field of view

At day 1, MDCK islands on the Si wafer had on average 3.5 cells per island with the largest cluster observed containing eight cells; the MDCK islands on the glass substrates has a significantly higher number of cells per island with nearly nine cells per cluster (Table 3.1), with the largest cluster containing 22 cells.

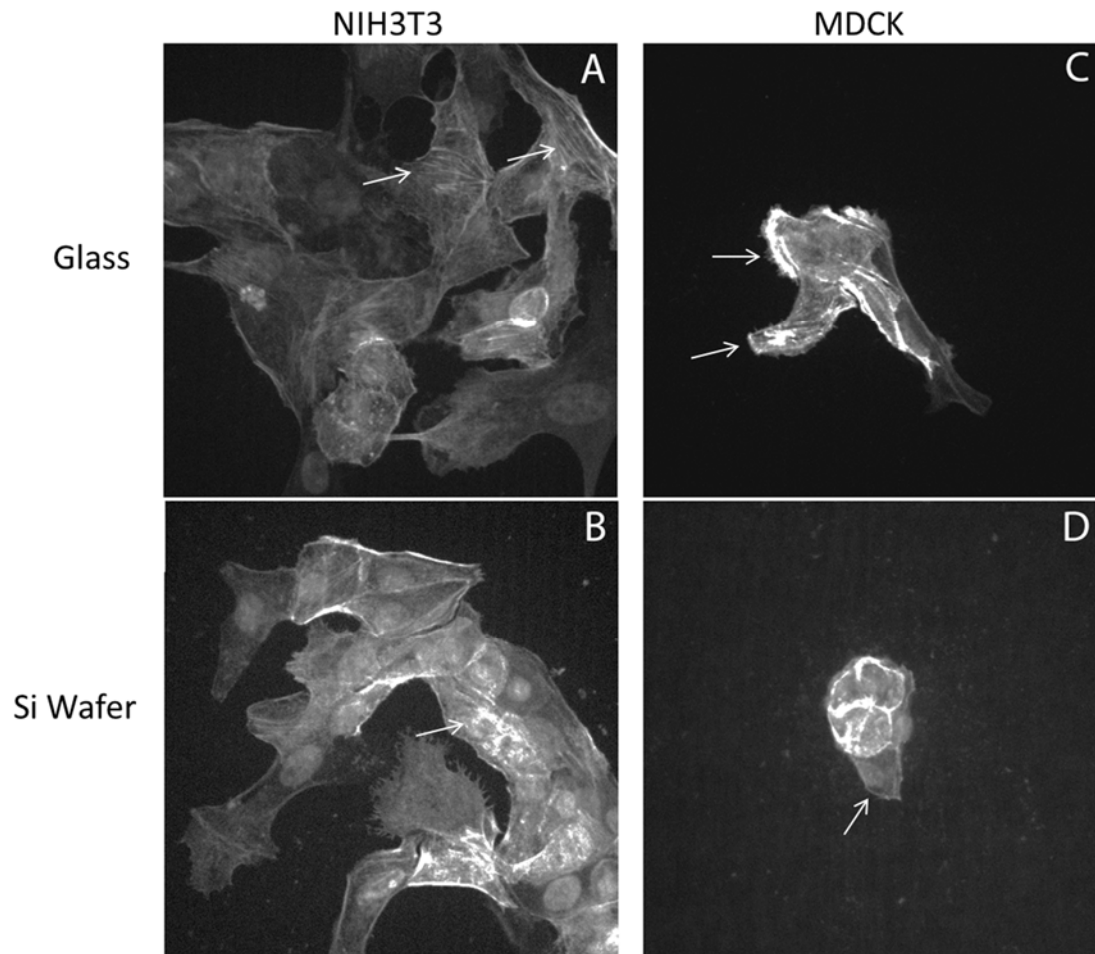


Figure 3.5. Morphology and F-actin Localization in Cells Grown on Glass and Si Wafer Plated Under “Low” Cell Concentration. F-actin labeled with Alexa488 Phalloidin, (A) Glass Cover Slip, NIH-3T3 cells at 1 day, note the present of stress fibers of f-actin along the axis of the cells (arrow); (B) Si Wafer, NIH3T3 cells at Day 1. Note the presence of accumulation of F-actin within the cell body (arrow) and the reduction of stress fibers. (C) MDCK cells grown on a Glass substrate, note the elongated morphology of the cells and the presence of filamentous actin long the leading edge of the lamellipodia of these cells (arrows); D) MDCK cells grown on Si Wafer, note the round appearance, cortical accumulation of actin, and the lack of any f-actin in the cellular extension (arrow). 40x Objective.

Also, we noticed that the actin cytoskeleton appeared altered in both NIH3T3 fibroblasts and MDCK epithelial cells when grown on Si wafers. Qualitatively,

actin appears brighter on the Si Wafer partially due to the reflection of the light from the mirrored surface of the Si Wafer, but also due to significant changes in the cellular organization and distribution of F-actin as measured by grey (Figure 3.5). When grown on a glass substrate NIH3t3 cells exhibit distinct stress fibers along the length of the cell (Figure 3.5A, arrow). When grown on “nanosmooth” Si Wafer, NIH-3T3 cells have a greatly reduced number of stress fibers and the accumulation of actin within the cell (Figure 3.5B, arrow). MDCK cells spread out more on glass than those on the Si wafer. MCDK cells grown on glass have cellular lamellipodia with a concentration of actin along the leading edge (Figure 3.5C, arrows). In contrast, the f-actin organization in MDCK cells grown on the Si wafer display a rounded morphology with a large amount of cortical actin and little showed fewer cellular extension, most interestingly the extensions that are present have little actin along the leading edge (Figure 3.5D, arrow).

III.4 Discussion/Conclusion

In this study we examined the role that nanoscale surface topology (or the lack thereof) plays in cellular growth and morphology. MDCK cells behaved differently on a nanostructured substrate (i.e. glass) with inherent nanostructures in the sub 10 nm ranges when compared to a nearly atomically flat substrate (i.e. Si Wafer). MDCK cells do not grow well on these surfaces at lower cell concentrations; cells form small round clumps or islands which slowly deteriorates over time (Figure 3.2, Table 3.1), instead of dividing and forming a

confluent sheet. The cell/substrate effect is an early event in the establishment of an epithelium as shown by the differences in the numbers of cells within each MDCK island initiated on a Si Wafer. Whether these differences reflect altered growth of the cells seeded onto this surface or alterations to the cell-cell and cell-substrate interaction (or some combination of the two) remains to be tested; nevertheless, these observations suggest a requirement for a level of cooperative interactions among the independent cells during the reestablishments of an epithelium from singly dissociated cells. All epithelial cells including MDCK cells require intercellular junctions, which could mean that without an appropriate amount of surface energy there may not exist enough cell-surface interaction to stabilize the cytoskeletal elements of these cells, leading to the limited cell growth on the Si Wafer observed. Our results demonstrate that MDCK cells cannot overcome the lack of physical/mechanical contacts on a featureless, ultra-flat surface. This is further demonstrated by the abnormal actin cytoskeleton in these cells, particularly the lack of f-actin in leading/spreading cellular extension such as lamellipodia. Our observation that the alteration to growth and morphology is ameliorated by an increase in the number of cells suggests that the cell-cell contacts, perhaps in a mechanical force generating manner, play a significant role in the organization and reformation of an epithelium. Although we observe a subtle change in the organization of actin in the mesenchymal NIH3T3 cells, we observe no alteration to attachment of these cells to the substrate or to the growth of these cells on either substrate.

Therefore, this may be a unique feature of a cellular epithelium. Previous work has shown that alteration to the mechanical stimulation ultimately results in changes to gene expression and that apart from the surface substrate, this mechanical stimulation involves both intra and extra cellular processes [24, 118]. The role that these different mechanisms play in the disruption of epithelial – i.e. whether it is due to alteration or regulation of the cytoskeleton in these cells or due to the alteration in the formation of a function and structurally stable extracellular matrix – remains to be tested. Nevertheless, the effect that topographical features on the order of sub 5 nm could have may be paramount for device design. Ignoring features on such a scale could alter intended function of the device or disrupt healthy cell growth and function.

CHAPTER IV

DIFFERENT CRYSTALLINE STRUCTURES DRIVE VARIATIONS IN ECM COMPOSITION AND MORPHOLOGY

IV.1 Introduction

Eukaryotic cells have very specific spatial requirements for forming adhesive junctions to surfaces and between cells and it is through these adhesion connections that cells communicate both chemical and mechanically [25]. Integrins need to be spaced 70nm apart in the plasma membrane to facilitate intracellular actin filament formation in focal adhesion contact [15] and at least four integrin molecules need to be within 60 nm to facilitate attachment [15]. Beyond cell-substrate attachment, other spatially-mediated interactions between the cell and the surface permit other cellular processes such as the remodeling of the cytoskeleton and motility [21]. For the past decade this fact has been repeatedly demonstrated as cellular interactions with nanostructured surfaces (NSS) guide cell differentiation, control cellular morphogenesis, and can even alter cellular viability [119]. Qualitative differences in the size and shape of the nanoscale features of the NSS controls these cellular interactions with the underlying substrate in subtly different ways [11, 120]. Nanoscale grooves promote cell polarization and elongation of fibroblast cells either along the groove or perpendicular depending on dimensions [10]. This nanoscale effect on cell

growth is even obvious in commonly used polymeric materials; anecdotally, the choice of tissue culture polystyrene dish has been known to play a significant role in governing proper cell behavior (growth, adhesion, differentiation) and recently it has been demonstrated that subtle alterations to nanotopography was the primary culprit of variation in cell behavior across various TCPS sources [76].

Cell/NSS interactions are mediated through a complex set of cellular mechanisms that includes direct adhesive interactions of the cell with the NSS substrate, as well as adhesive interaction between the deposited extracellular matrix. The formation and maturation of focal adhesion complexes plays a central role to these nanoscale interactions with the substrate [12]. Cell-substrate interactions are also mediated by protein-protein interactions, such as integrin/ECM interactions, as integrin mediated signaling is required for normal growth [26]. Moreover, interactions of proteins and NSS also indirectly control and govern cell growth and differentiation. Although, the rules that govern protein adsorption are just beginning to be described. Recent work has shown that nanoscale features can influence the adsorption and organization of proteins [50]. However, the scale upon which cells can react remains vague as do the responses of cells. Although we know that certain protein motifs (RGD) are on the order of sub nanometer scale – the type of reaction that cells have to subtly different features remains undetermined. We are interested in understanding the limits of nanoscale interactions on biological material, both cells and proteins, and begin to elucidate the cellular responses to these fine scale differences. We

chose to investigate the effects of growth and morphogenesis of an epithelial cell line (MDCK cells) on three different SiO₂ substrates that represent a range of organizations. Silica/SiO₂ is a common material that has been shown to interact biological in a number of different ways and is the material of choice for the semiconductor industry and a possible component for many bioelectronics MEMS and NEMS devices. While there is some literature regarding the role that crystalline organization of a TiO₂ material has in both protein adsorption and cellular adhesion, little work has been done with silicon.

IV.2 Materials and Methods

Cell Culture: MDCK cells were cultured with DMEM/ High Glucose (Hyclone Cat no. SH30022.01). Cells were transferred using 1x Trypsin/EDTA (MP #1689149) and Cell Stripper (Corning REF:25-056-CI). For 25 cm² flasks we used 1.5 milliliters of each for 25 min at 37 degrees C. For 75 cm² we used 3 milliliters of each for 25 min at 37 degrees C. Cells were diluted at 40X for each experiment and were passed between 65-75% confluency.

Surface Preparation: Three specific silicon substrates were used: glass coverslips (GCS; Globe Scientific, Inc., Item #1401-10), <111> crystalline silicon wafer (111-SiW; Ted Pella, Inc., Prod. No. 16010), and <100> crystalline silicon wafer (100-SiW; Ted Pella, Inc., Prod. No. 16015). Surfaces were cleaned together with a standard RCA-1 cleaning procedure. Briefly, surfaces were washed in acetone for 15 min. at 70 degrees, washed with methanol for 5 min. at

room temperature, and then washed in a 1:1:5 solution of 30% hydrogen peroxide, 30% ammonium hydroxide, and DI Water for 15 min. at 70 degrees C. Surfaces were also cleaned with an oxygen plasma cleaner (South Bay Technologies, Inc., PC-2000) in order to control for possible residue after the RCA-1 cleaning procedure. Surfaces were washed for 15 min. in Acetone, then 5 min. in Methanol and washed in DI Water. After the initial solvent wash, surfaces were then cleaned with O₂ plasma for 15 min. at 100W.

AFM Imaging: AFM images were obtained using an Agilent 5600 LS AFM.

Surfaces were imaged using SiN₄ tips (Ted Pella – SINI-30) with a labeled force constant of 0.2 N/m. Measurements of the spring constant using the thermal-K tool available in Pico View 1.14 (Agilent) software gave values of k within the expected range of 0.2 N/m +/- 0.07 N/m. Deflection sensitivities were measured to be 75 nm/V +/- 20 nm/V for all experiments. Surfaces were imaged at 1 line/s at 2 nN with a 25 μm² field of view. Proteins were imaged using tapping mode with a tip of spring constant 40 N/m (Ted Pella, Inc., Prod. No. TAP300AL-G-W). 10 μm images were taken at 1 line/s. Images were then processed using Pico View v.1.4. Adsorption was measured by counting structures larger than 10 nm, which would be expected as a minimum size of the proteins.

Confocal microscopy: MDCK cells cultured as described above on GSC or on <111> or <100> wafers for four days and then fixed in 4% formaldehyde in 1X Phosphate buffered Saline (pH7.4) for 20minutes. Cells were then labeled with mouse primary monoclonal antibodies (1:500 dilution in 1X PBS, 1% BSA, 0.1%

Triton): E-cadherin (rr1; Developmental Studies Hybridoma Bank) [121], type II collagen (II-II6B3; Developmental Studies Hybridoma Bank) [122], collagenase pro-enzyme (H18G8; Developmental Studies Hybridoma Bank) [123], fibronectine III-15 (13G3B7; Developmental Studies Hybridoma Bank)[124], and S-laminin (C4; Developmental Studies Hybridoma Bank) and a goat ant-mouse secondary antibody (Jackson labs, 1:2000 dilution). Cells were also counter labeled with Hoescht to detect the DNA/nucleus (Molecular Probes/Lifetechnologies) and alexa 488 phalloidin (Molecular Probes/Lifetechnologies) to detect filamentous actin. All images were collected using Zeiss Observer Z.01 spinning disc confocal with Axiovision software. All images were collected using the same exposure times and laser settings. Densitometry data was collected from individual frames using the Interactive Measurement application within Axiovision. Densitometry data was statistically analyzed using Microsoft Excel software, specifically the student ttest function; parameters were set as 1 tail, unpaired. MDCK cells do not express Fc Receptors

Cell Wash Assay: In order to probe the quality of adhesion on each surface, a hydrostatic wash was performed on cells using a mechanical pipette. Cells were cultured on each surface for 24 hrs. Live cells were then stained with Heochst for 5 minutes and then immediately counted. Surfaces were removed from the microscope, washed with 300 ul of 1x PBS at the highest setting for the pipette

and then reimaged. Experiment was repeated 3 times. Student ttest was used to determine significance; parameters were set as 1 tail, unpaired.

IV.3 Results

We measured protein absorption and the growth of epithelial cells on three different forms SiO₂ surfaces: amorphous glass cover slips (GCS), <100>, and <111> silicon wafers. The variation between the surface properties of these three materials is subtle and interesting. Although the starting material for the two crystalline substrates is pure Silicon crystalline wafer, a native and self-limiting oxide layer forms almost immediately upon contact with atmospheric oxygen [125]. In this manner we can generate a range of substrates that share similar compositions. We examined the surface morphology of the cleaned SiO₂ surfaces using AFM. All three surfaces are extremely flat as expected (Figure 4.1). The <100> substrates exhibit the ultrafine scale difference in nanotopography of less than 0.5 nm delta Z compared to 1.5 nm delta Z of GCS and <111> substrates. Amorphous glass cover slips (GCS) and the <111> wafers share a similar morphology with both presenting a regular sets of wave-like contours across the surface (Figure 4.1), while the <100> Si wafer are relatively featureless.

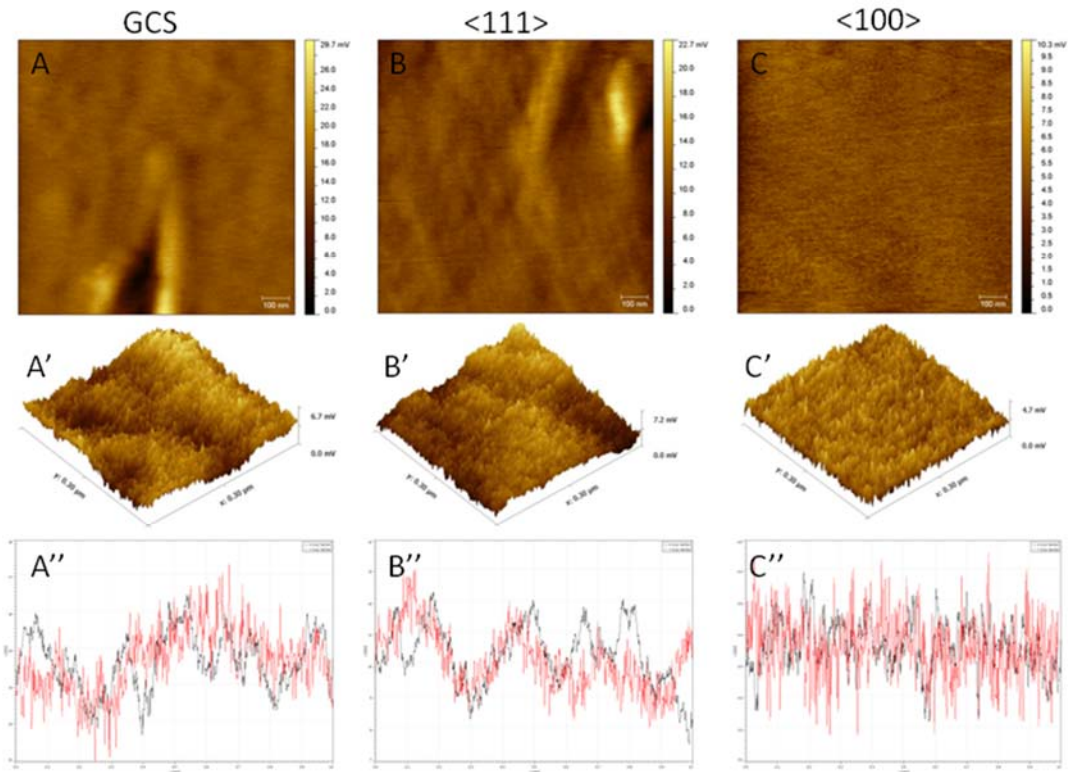


Figure 4.1. Atomic Force Micrographs of GCS, <111>, and <100> Substrates Used in this Study.

AFM images of 100-SiW did not show discernable variations in topography were as each the GCS and 111-SiW show wavy patterns. The largest features resolved were approximately 1.5 nm. Wavy features were measured to be less than 1 nm but consistent across the surface.

In order to characterize the differences in surfaces we used Raman Spectroscopy to verify the similar composition of each surface. As expected, the Raman data showed no differences between <111> and <100>, which are composed of SiO₂ at the surface. We used an ellipsometer to measure the thickness of the oxide layer for the <111> and <100> silicon wafers. We measured the oxide layer of <111> silicon wafers to be 9.7 ± 2.5 nm, with the <100> silicon wafer measured as 10.1 ± 2.1 nm. Contact angle measurements

were taken to demonstrate variability in surface energy. Initial contact angle measurements on each surface using DI water and complete media (DMEM with FBS) had angles less than 10 degrees demonstrating a very hydrophilic surface. This was probably due to residual effects from cleaning the surfaces because surfaces after 24 hrs. were tested and had contact angles of 27.3 degrees for GCS, 13.8 degrees for <111>, and 10.1 degrees for <100>.

	GCS-AP	111-AP	100-AP	GCS-P	111-P	100-P
GCS-AP		0.0350889	0.049019399	4.3327E-05	0.0034151	0.020303863
111-AP			9.56E-05	0.004347676	0.19017794	0.379374155
100-AP				3.6951E-08	4.8872E-07	4.78078E-05
GCS-P					0.01810178	0.009935083
111-P						0.301855235
100-P						
	GCS-Nt	111-Nt	100-Nt	GCS-H	111-H	100-H
GCS-Nt		0.03317385	0.000186397	0.107271896	0.00072767	0.001258293
111-Nt			0.020570804	0.004053188	0.07552172	0.110319171
100-Nt				9.89783E-05	0.06309015	0.082843939
GCS-H					0.00024619	0.000336832
111-H						0.401455014
100-H						

Figure 4.2. Statistical Significance Between All Surfaces Used.

Surfaces are labeled as glass cover slip (GCS), plasma cleaned glass cover slip (GCS-P), silanized glass cover slip (GCS-H), <111> silicon wafer (111), plasma cleaned <111> silicon wafer (111-P), stripped and regrown native oxide <111> silicon wafer (111-Nt), silanized native oxide <111> silicon oxide (111-H), <100> silicon wafer (100), plasma cleaned <100> silicon wafer (100-P), stripped and regrown native oxide <100> silicon wafer (100-Nt), and silanized native oxide <100> silicon wafers (100-H). For each AP and P group n=20. For each Nt and H group n=10. Red font indicates statistical significance (p<0.05).

One concern was that the surfaces I examined were qualitatively different

– one set contained an uncontrolled oxide layer and the other had controlled

oxide growth. The rationale behind the experiments in Figure 4.2 was to determine whether the differences I observed were a result of the differences in these oxide layers or due to some other unknown effect. By growing the oxide layer I was able to ensure the composition of the oxide layer, which was impossible for the as-purchased surfaces. Each surface was compared as shown in Figure 4.2. Top chart indicates comparisons between GCS, 111-SiW, and 100-SiW surfaces with the as-purchased oxide layer, cleaned by hydrogen peroxide and ammonium hydroxide (indicated by the -AP suffix) and cleaned by acetone, methanol, and oxygen plasma (indicated by -P suffix). The bottom table indicates comparisons between GCS, 111-SiW, and 100-SiW where the as-purchased oxide layer was stripped and regrown (indicated by the -Nt suffix), and regrown oxide layers were coated with HMDS (indicated by the -H suffix).

Each of the as-purchased and plasma treated surfaces, except for the 100-AP, demonstrated an increase in the number of cells at 4 days compared to GCS-AP. Interestingly, the GCS-Nt and GCS-H both showed a greater number of cells compared to the 111 and 100 orientation of regrown native oxide layer and nonpolar (HMDS treated) surfaces. This could indicate that the 111-AP orientation is the most favorable surface for cellular adhesion having both favorable surface chemistry and topography, or some other unique aspect (ambient conditions from manufacturer, etc), as all other surfaces had less cells than their corresponding GCS control. Also, the plasma treatment removed the differences observed between the 111 and 100 orientations, which may suggest

that some unknown, uncharacterized organic material was removed. Similar effects were observed for the silanization of the regrown native oxide layers. This may suggest that the variations in MDCK growth observed between these two substrates with different crystalline orientations is driven primarily by surface chemistry. Furthermore, the plasma treated GCS demonstrated an increased number of cells compared to as-purchased GCS, which again may suggest that there was some unknown, uncharacterized organic material that was removed and the origin of the substrate matters. This was also true for the plasma treated 100 orientation compared to the as-purchased 100 orientation. This trend was not observed for regrown native oxide layers that were silanized, meaning 100-Nt showed no significant differences from 100-H, and likewise for 111-Nt to 111-H. This could indicate the favorable effects of the plasma treatment, or removal of some uncharacterized organic material, suggesting plasma cleaning could be used as a way to make surfaces more favorable for adhesion. Also, the 111-Nt and 100-Nt surfaces showed less cellular growth than their corresponding GCS control. This trend was also seen for the 111-H and 100-H compared to the corresponding GCS control. This could indicate a slight topographical effect between surfaces, in tandem with the noted surface chemistry differences, as the general trend of GCS having a greater number of cells compared to the Si Wafer was consistent across all controlled surfaces.

In general, the highest surface energy and roughest surfaces supported the highest observed cellular growth. The common thread was that GCS

supported the largest cell growth numbers compared to Si Wafers in all cases except the 111-AP, which suffers from uncontrolled conditions, such as ambient temperature, atmospheric contaminants, etc., in oxide layer growth. As the growth rate between GCS and Si Wafer were consistent, this could suggest that topographical variations play some role in observed effects. Also, the variations between cell growth on different Si Wafer orientations was eliminated by treating the surface with both plasma cleaning and HMDS.

To investigate the reaction that the MDCK cells have to GCS, <111>, and <100> substrates we examined the growth of the cells, cell viability, alteration to cell morphology, and growth habit. Previous studies didn't show any change to the viability of MDCK cells grown on GCS or silicon, but we did observe significant differences in the growth of MDCK cells.

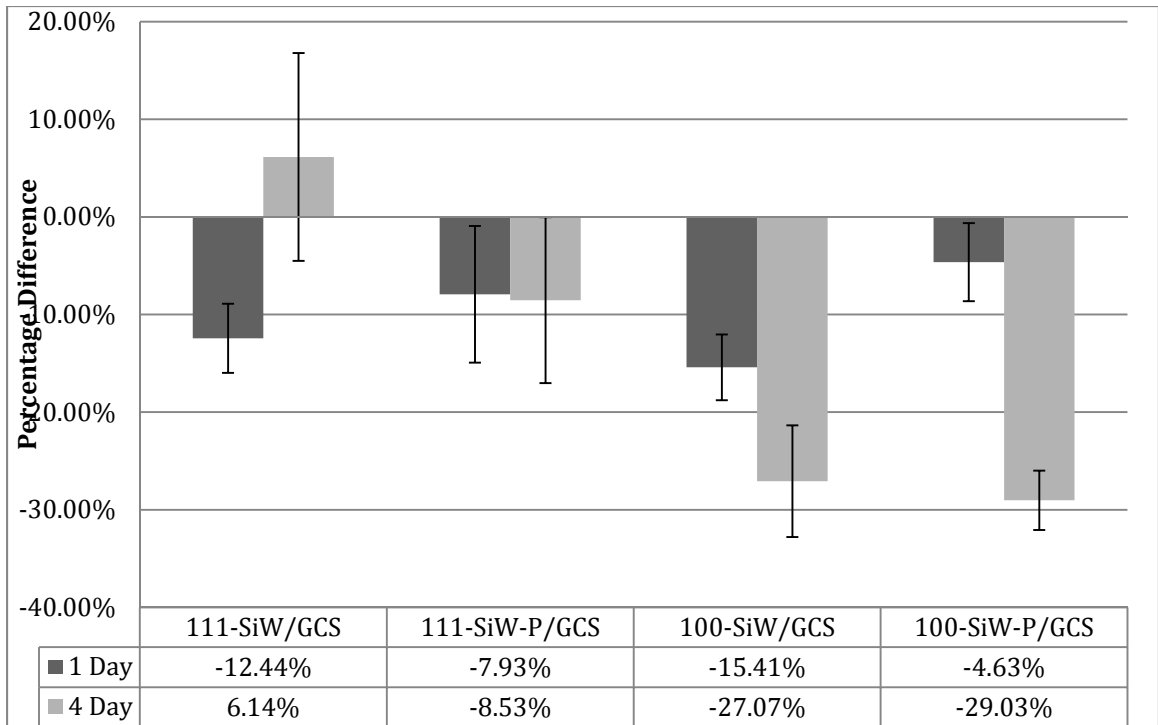


Figure 4.3. Epithelial Cell Growth on GCS, <111>, and <100> Silicon. MDCK 1 day (dark grey) & 4 day (light grey) growth compared on each surface: 100-SiW, and 111-SiW compared to GCS; surfaces were cleaned with standard RCA-1 cleaning, and plasma cleaning (denoted by -P beside surface name). Values are given as percent differences to GCS. The 100-SiW Growth was the only consistent statistically significant difference observed (n=5, p<0.05).

There is significant reduction of the MDCK cell growth when on <100> silicon wafers when compared to <111> silicon wafers and amorphous glass coverslips (Figure 4.3). The reduction in the rate of growth was observed both on RCA-1 cleaned surfaces and plasma cleaned surfaces (see methods) demonstrating that it was inherent differences in the <100> surfaces themselves and not some residual effect of the substrate preparation.

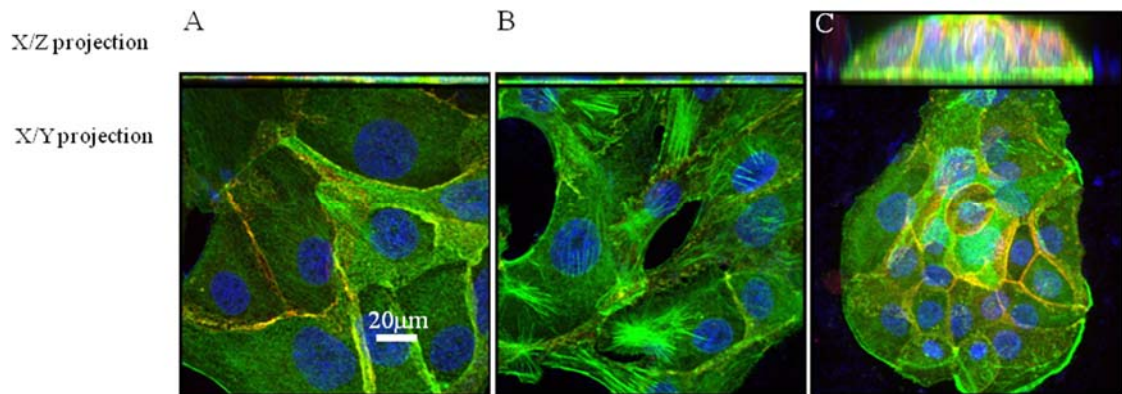


Figure 4.4. Confocal Micrographs Demonstrating the Growth Habit and Morphology of MDCK Cells Cultured on GCS and Si Wafers, $\langle 111 \rangle$ and $\langle 100 \rangle$. The cells are triple labeled with Hoescht (blue), anti-cadherin (red) and Alexa 488 phalloidin (green). Scale bar $20\mu\text{m}$. The micrographs are 2D projects in the X-Z (top panel) and X-Y planes (bottom panel). (A) MDCK cells cultured on GCS adopt a sheet squamous epithelium-like morphology. This is demonstrated by short height of the cell in the X-Z projection (top) and the flat spread out cells in the sheet in the X-Y (bottom). (B) MDCK cells cultured on $\langle 111 \rangle$ substrate has a similar flat morphology to that exhibited by GCS culture MDCK cells, although other morphology such as clustering (Table 4.1) are also observed. Nevertheless, the epithelium is flat (B, top panel). (C) The epithelium of MDCK cells cultured on $\langle 100 \rangle$ substrate has a striking appearance. The cells grow exclusively in a tight colony (bottom panel) and are significantly taller when compared to either CGS (A) or $\langle 111 \rangle$ (B) cultured MDCK cells.

While the MDCK cells grew more slowly on $\langle 100 \rangle$ (Figure 4.3), the MDCK epithelia grown on $\langle 100 \rangle$ wafers expressed a strikingly different morphology (Figure 4.4). MDCK cells grown on glass cover slips and $\langle 111 \rangle$ wafers generally form a flat continuous sheet of cells in a squamous-like epithelium that average in height between 2.5 and $3.5\ \mu\text{m}$ (Table 4.1).

Table 4.1. Morphology and Growth Habit of MDCK Cells on GCS, <111>, and <100> Substrates.

Surface	Growth habit (%)	Average Cell height (μm)
Glass cover slip	Sheet, 100%, n=44	2.4 \pm 0.5
Si <111> wafer	Sheet (72%), clustered (28%), n =43	3.9 \pm 1.8*
Si <100> wafer	Clustered 100%, n=45	13.9 \pm 7 **

* difference from GCS highly significant, P value <0.001

** difference from both GCS and <111> highly significance P value, <0.001

However, MDCK cells cultured on <100> wafers form dense colonies of a taller cuboidal-like epithelium with an average cell height of 13.9 μm – roughly 5-6 times taller than MDCK cells grown on <111> wafers and GCS (Table 4.1).

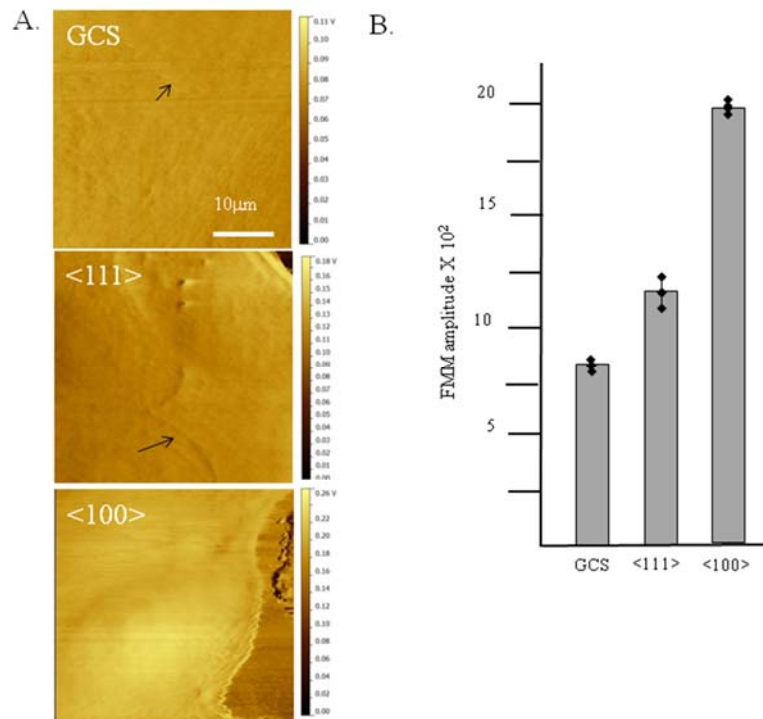


Figure 4.5. AFM Force Amplitude Images of MDCK Cells Cultured on GCS, <111> and <100> Substrates. (A) AFM micrographs of MDCK cells cultured on GCS (top), SiW-111 (middle), and SiW-100 (bottom). The heat map ranges from light to dark with the lighter colors showing a greater deflection (i.e. greater rigidity of the cell). Note the ability to discern cell outlines (Arrows in GCS and <111> micrographs). B) Graphical description of the force amplitude images. The SiW-100 surface had the highest average amplitude with significantly higher value throughout the cell when compared to SiW-111 and GCS ($p < 0.001$).

To determine whether MDCK cells cultured on GCS, <111>, and <100> substrates have altered mechanical properties, we examined the rigidity of live MDCK cells using atomic force microscopy. AFM approaches have been used to examine adhesive forces in bacterial biofilm formation [126, 127], changes in the yeast cell wall elasticity as a result of heat shock [128], genetic cell wall studies in yeast [129], and to study the mechanical aspects of apoptosis [130-133]. More

recently such AFM force spectrographic techniques have allowed the characterization of membrane blebbing in live motile cells [134] and adhesion forces in cardiac fibroblasts [135]. Our study is the first to examine the mechanical aspects of a living epithelium. In this study we used the deflection of an AFM probe (SiN; k measured at 0.03 N/m) to demonstrate the rigidity of the cell as it was imaged; simply put the greater the deflection of the AFM probe's tip the more rigid the sample (Figure 4.5, A, B). Using this we clearly show that the tall colonial MDCK cells that grown on $\langle 100 \rangle$ substrates are nearly twice as rigid as MDCK cells cultures on $\langle 111 \rangle$ substrates and more than twice as rigid as MDCK cultures on GCS substrates (Figure 4.5, A, B)

To investigate the quality of adhesion on each surface, a wash assay was performed confirming that MDCK cells grown on $\langle 100 \rangle$ wafers have reduced affinity for the substrate after four days of culture (Figure 4.6), although there is no difference in cell-substrate adhesion among all substrates after one day of culture. MDCK cells cultured on $\langle 100 \rangle$ exhibited less adhesion to the surface substrate when compared to either GCS or $\langle 111 \rangle$ substrates as determined by the greater loss of the number of cell per field of view after a gentle wash (Figure 4.5). On average both CGS and $\langle 111 \rangle$ substrates had similar number of cells per field of view prior to washing (GCS, 75.2 ± 33 ; $\langle 111 \rangle$, 74.5 ± 22), while $\langle 100 \rangle$ has slightly less (58.8 ± 29), which reflects the slightly reduced growth rate of MDCK cells on $\langle 100 \rangle$ substrates. After washing, we observed reduced amounts on all three. Again, we observe a similar reduction in both GCS and $\langle 111 \rangle$, 22%

and 28% fewer cell respectively. However, we observed a significant 48% reduction in the number of MDCK cell on <100> surfaces, demonstrating lower adhesion of these cells to this surface.

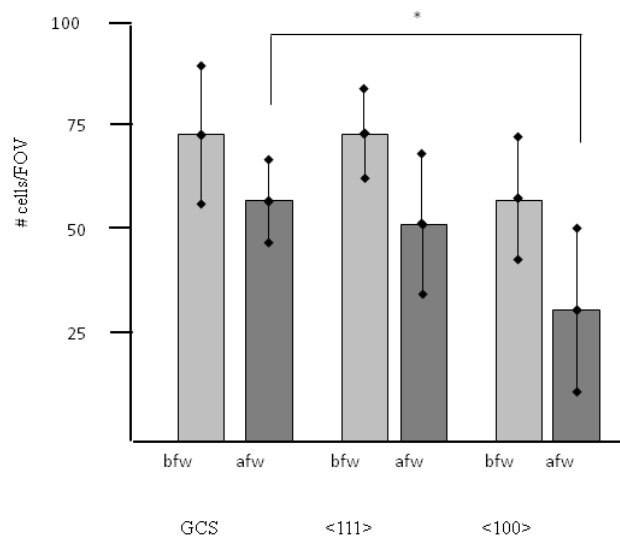


Figure 4.6. Cell Wash Assay on MDCK Cells Cultured on GCS, <111> and <100> Substrates.

MDCK cells were cultured on substrates for 4 days and subjected to a series of hydrodynamic wash cycles. Cells were then fixed and labeled with Hoechst and the number of cells per field of view were counted before and after washing using confocal microscopy under the 20X objective. In each case a similar fraction of cells were observed to be removed from both GCS and <111> substrate after the wash, however, MDCK cells cultured on <100> demonstrated significant reduction of cell/FOV after washing when compared to either GCS or <111> cells. n=20, * represents p<0.05.

To determine whether these changes in adhesion and morphology reflect a change in the organization of the actin cytoskeleton we examined organization of basal actin. Adherent cells, both epithelial and fibroblastic, form characteristic bundles of actin called stress fibers that are indicative of adherence of the cell to

the surface substrate through integrin based complexes called focal adhesion contacts [18]. To examine these basal actin structures in MDCK cells cultured on GCS, <111> and <100> substrates, we labeled cells with 488 Alexa phalloidin and examine the actin localization using confocal microscopy. By looking at the first few confocal sections above the substrate we can observe basal actin location in the context of cell-substrate adhesion. We observed 40% of the MDCK cells grown on GCS substrates having long and well organization stress fibers (LoSF, i.e. fibers that extent along one axis in the cell), 12% of the cells having shorter, less organized stress fibers (sdSF, i.e. fibers that had multiple directions in the cell) and 48% of the cells without clearly defined stress fiber (Figure 4.7, Table 4.2).

Table 4.2. Basal F-Actin and Adherens Junction Organization in MDCK Cells Cultured on Glass and Si Wafers.

Surface	n	Basal actin organization			AJ organization		Cadherin levels	
		loSF	sdSF	No SF	% diffuse	% tight	Average Grey value	% change from GCS
Glass cover slip	224	40%	12%	48%	57% (n=43)	43%	5729±1539	-
Si <111> wafer	85	34%	28%	38%	64% (n=44)	36%	6157±2828	103%
Si <100> wafer	133	0%	59%	41%	9% (n=45)	91%	8997±1772*	150%*

loSF – long and organized stress fibers

sdSF – short and disorganized stress fibers (i.e. short stress fibers with multiple orientations)

No SF – no distinct stress fibers

* difference from both GCS and <111> , highly significant P value, <0.001

In MDCK cells cultured in <111> wafers we observed an increased amount of SDSF and a slightly reduced amount of cells with longer stress fiber (Figure 4.7; Table 4.2). However, in MDCK cells grown on a <100> substrate we observed a

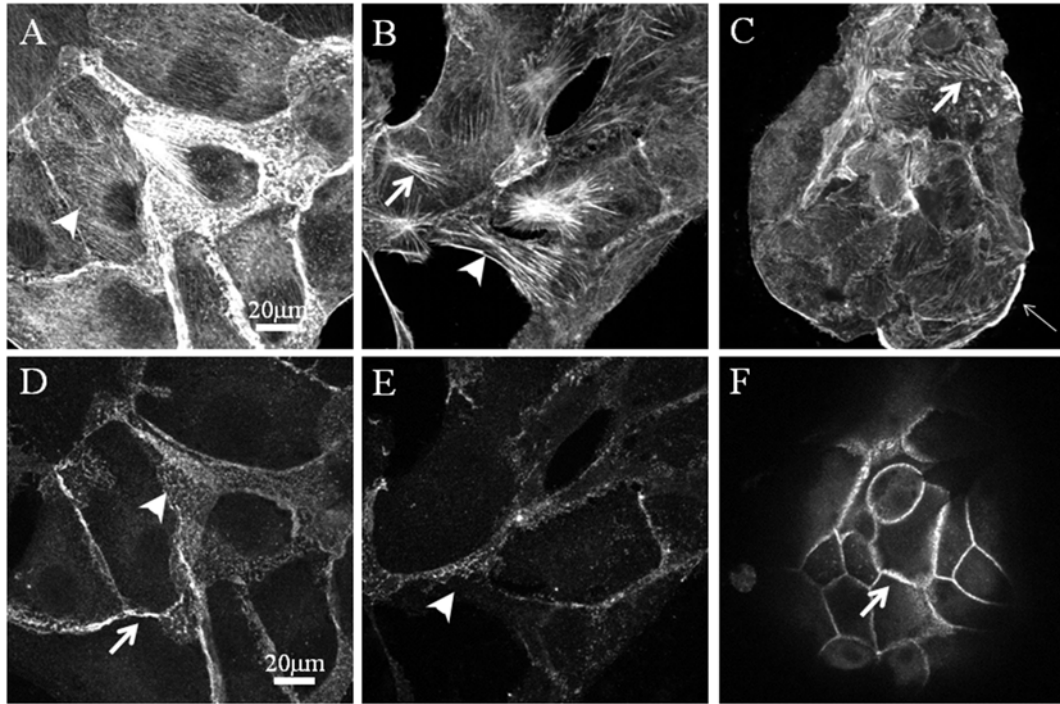


Figure 4.7. Basal Actin and Adherens Junction Organization in MDCK Cells. Cells were cultured on GCS (A, D), $\langle 111 \rangle$ (B, E) and $\langle 100 \rangle$ (C, F) substrates. A-C) Basal F-actin organization in MDCK cells as shown by Alexa 488 phalloidin; D-F) adherens junction organization as shown by localization of cadherin. MDCK cells cultured on GCS shown a range of basal F-actin morphology, the most pronounced are the long stress fibers that are present in roughly half the cells (A, arrow head; Table 4.2). These same MDCK cells have adherens junctions that exhibit a range of morphologies including diffuse junctions, which are characterized by punctate localization of the cadherin (D arrow) and also tighter, more organized junctions (D, thick arrowhead). MDCK cells cultured on $\langle 111 \rangle$ substrates have a range of basal f-actin and adherens junction morphologies. Basal actin of MDCK cells cultured on $\langle 111 \rangle$ form of long stress fiber similar in appearance and organization to those seen in GCS cultured cells (B arrowhead) as well as smaller, less organized stress fiber bundles (B thick arrow). As with GCS cultured cells, the adherens junctions show a similar range of morphologies that is dominated by the diffuse, punctate localization of cadherin (E arrowhead). MDCK cells cultured on $\langle 100 \rangle$ exhibit different organizations of basal actin and adherens junction. Most of the organized F-actin is found in smaller disorganized bundles (C arrowhead), and the edge of each colonies is rimmed with a thick layer of cortical actin (C, thin arrow). Moreover, MDCK cells cultured on $\langle 100 \rangle$ have highly organized adherens junctions as defined by the intense localization of the cadherin (F, arrow).

dramatic loss of all long and organized stress fibers with only short and multi-oriented fiber being present (Figure 4.7 C, arrow). This result strongly suggests that the interaction of the MDCK cells with <100> wafers is distinct and different from either the GCS /MDCK or <111> /MDCK interactions.

Epithelial cells have cell to cell adhesive interactions that are mediated through supramolecular protein complexes called adherens junctions [18]. Epithelial cells use these adherens junction not only to maintain mechanical stability and control over the epithelium but also to direct and regulate intracellular signaling pathways. The adherens junctional complex is composed of both a transmembrane protein from the cadherin family, which serves as the connection between neighboring cells within the epithelium; the intracellular cytoplasmic domain of the cadherin binds multiple adaptor molecules that bind the cortical actin cytoskeleton and function to maintain the mechanical and physical robustness of the linkage between cells [18, 31, 136]. Changes in the levels and or type of cadherin molecules are indicative of both qualitative and quantitative properties of the adherens junction. For instance, increased cadherin expression has shown to be directly associated with stronger cell-cell adhesion [137, 138]. In another classical example, during vertebrate neural tube formation the induction of N-cadherin expression, which has an inherently stronger homophilic binding than e-cadherin, results in a conversion of the squamous ectodermal epithelium to a columnar neural epithelium [18]. To determine whether culturing MDCK cells on <100> substrate results in an alteration to the

cell-cell adherens junction, we examined the organization of the cell-cell contacts using an antibody directed against the cadherin type expression in MDCK cells. We also observe significant quantitative and qualitative differences in the organization of the adherens junctions in MDCK cells grown on <100>; 91% of all the adherens junction in MDCK cells grown on <100> have well organized adherens junctions that extend the entire height of the cell (Figure 4.7 C, arrow). In contrast, the adherens junctions of cells grown on either GCS or <111> substrates are diffuses (Figure 4.7, A, B). Moreover, there is a significant increase in the amount of cadherin per unit area of adherens junction when compared to either cell grown on CGCS or <111> substrate as determined by densitometry (Table 4.2).

Since we observed significant changes in the manner that the MDCK cells interact with their substrate as well as with each other, we tested whether there was differential protein absorption, specifically ECM protein absorption to these different surfaces. The ECM is a complex material that is secreted from cells, in the case of an epithelium, this matrix is often found on the basal lateral face [18]. The ECM serves as a substrate for the growth and maintenance of epithelial cells as well as serving as a bulletin board for guidance cues and signals for migrating cells [18]. The ECM is composed of several major families of proteins including collagens, laminins, and fibronectin proteins. To determine whether ECM proteins interact with the different SiO₂ substrates we evaluated the adsorption of ECM proteins (collagen, laminin, and fibronectin) using a chemiluminescent

surface analysis of ECM protein adsorption, an AFM based technique, and using fluorescently labeled proteins.

Immunological techniques have been used to detect protein localization on engineered substrates. To examine the binding of ECM proteins to GCS, <111>, and <100> substrates we performed a modified dot blot technique in which substrates were incubated with cell culture medium containing fetal bovine serum.

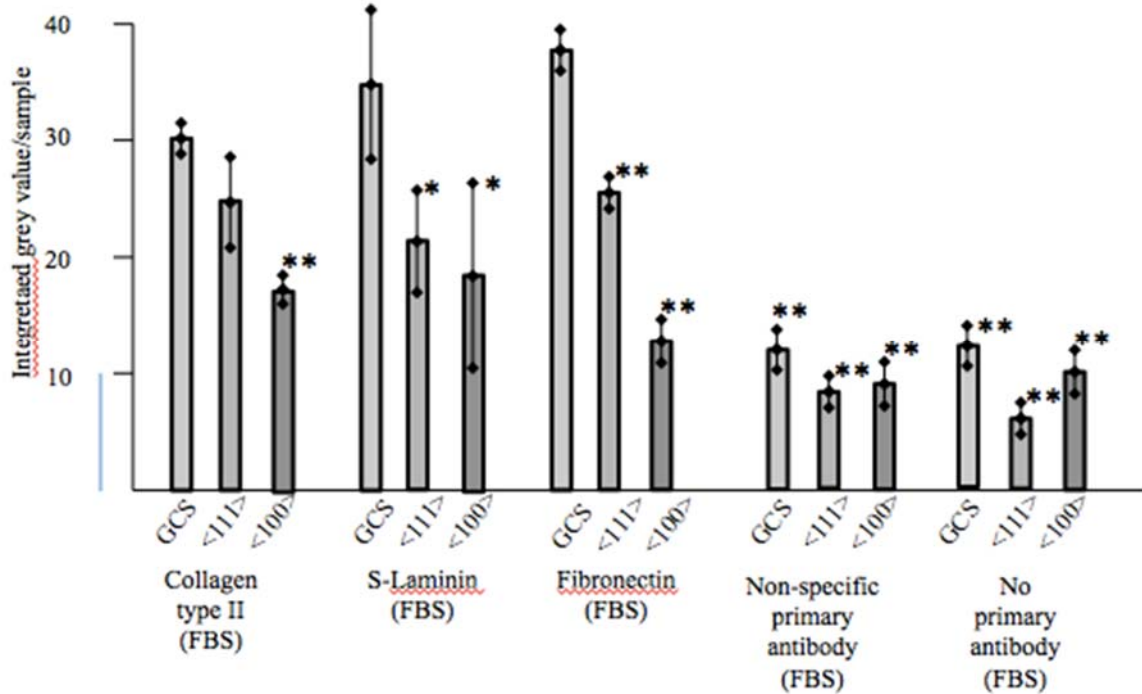


Figure 4.8. Chemiluminescent Surface Analysis of ECM Protein Adsorption on GCS, <111>, and <100> Substrates.

Protein adsorption was measured using immunological detection. Primary antibodies directed against collagen, s-laminin, and fibronectin were used with a secondary antibody with horseradish peroxidase. In each case the GCS demonstrated the greatest amount of protein adsorption compared to the <111> and <100> surfaces. * denotes $p < 0.05$ and ** denotes $p < 0.001$.

These treated surfaces were then subjected to an immunological detection technique using antibodies directed against collagen II, laminin, or fibronectin. Then, we measured the amount of binding using chemiluminescence production via a horse radish peroxidase conjugated secondary antibody. We observed differences in ECM protein adsorption to the different substrates and not all substrates interacted with the different proteins in a similar fashion. We observed a decrease in collagen II, laminin, and fibronectin adsorption on <100> substrates when compared to GCS, <111> as shown in Figure 4.8.

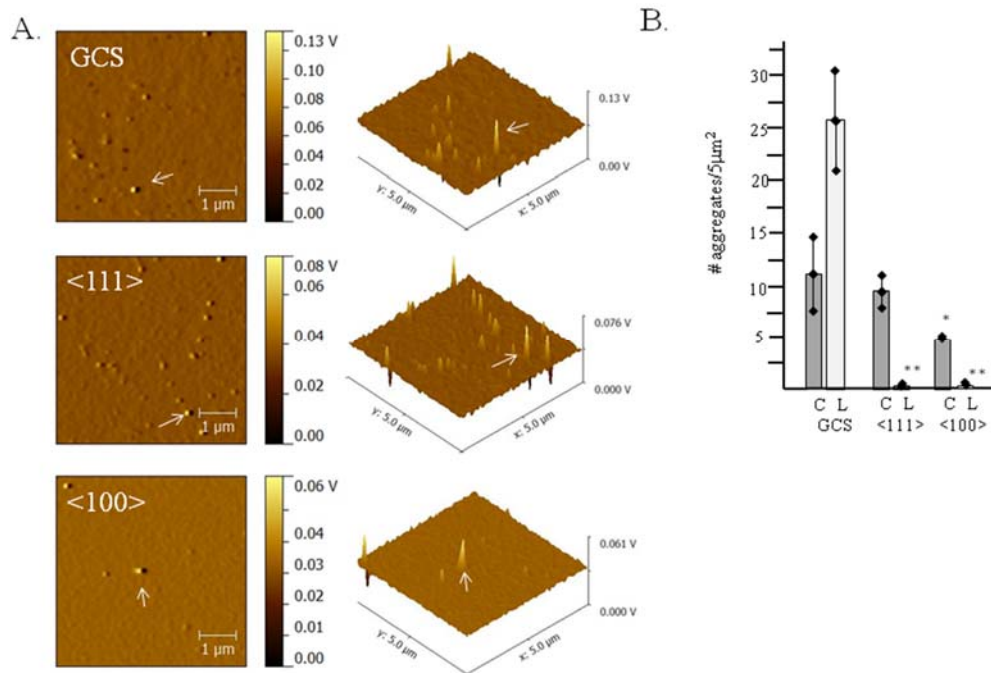


Figure 4.9. AFM Analysis of ECM Protein Aggregates Adsorbed on GCS, <111>, and <100> Substrates.

Prepared substrates were treated with purified collagen and the surface adsorption of the collagen was recorded using AFM (A) AFM micrographs of collagen aggregates on the substrates GCS (top,) <111>- (middle) <100> (bottom). The first column are top down images of the surfaces after adsorption, the second columns are angle views of the aggregate on the surface. The arrows note the position of aggregates on the surface and an example of what was quantified. B) A graph of the quantification of the number of aggregated per 5 μm² area on each surface. Two different ECM proteins were examined collagen II (C) and s-laminin (L). The number of protein aggregates as noted by the arrows in (A) were counted in ten fields and their average with standard deviation noted. GCS substrates showed significantly more collagen aggregate adsorption than the <100> substrate and significantly more laminin than both <111> and <100> substrates.

To complement the previous experiments we also directly examine the binding of purified ECM proteins to GCS, <111>, <100> substrate using atomic force microscopy. We treated each surface with purified collagen (0.003 μg/ml) or laminin and then examined these surfaces using AFM contact mode to image

protein deposition onto surface (Figure 4.9). AFM analysis of the surfaces involved counting the number of features attached to the surface per unit area. We observed significantly less protein of any type on <100> substrate when compared to GCS and <111> substrates (Figure 4.9). We also examined the adsorption of fluorescently labeled extracellular matrix proteins fibronectin and laminin, and used confocal microscopy to measure mean fluorescence per unit area. In a similar fashion to protein adsorption experiments above, we observed reduced levels of fluorescent proteins on both <100> and <111> substrates when compared to the GCS, with less on the <100> substrate when compared to <111>.

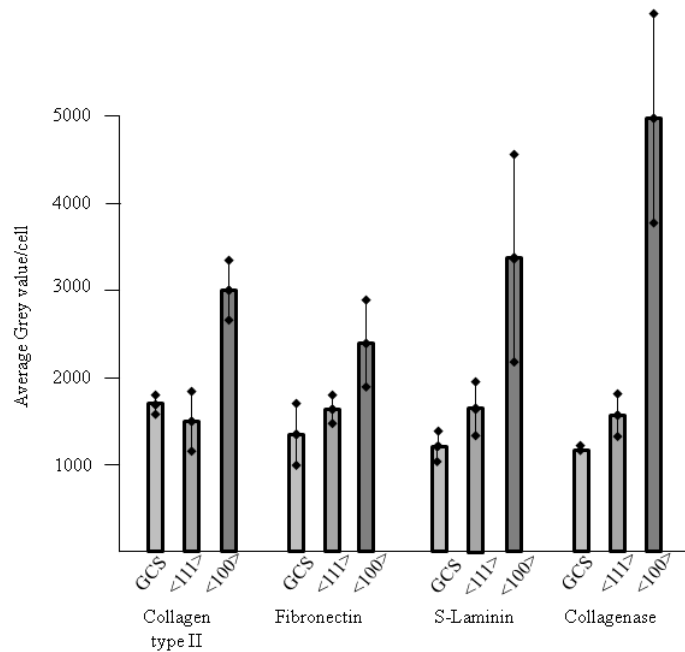


Figure 4.10. ECM Protein Expression Levels in MDCK Cells Cultured on GCS, <111>, and <100> Substrates.

Protein level expression was determined using densitometry analysis of confocal images of cells probed using monoclonal antibodies for collagen II, fibronectin, s-laminin, and collagenase. The densitometry data was collected from the basal portion of the cell, three confocal sections above the substrate and data for each cell was defined and delineated by actin (see figure 9 A,B, C for details). Densitometry data for each cell was collected, statistically analyzed, and graphically depicted. MDCK cells cultured on <100> substrates show significant increase in all the expression of all ECM proteins.

These results suggested that MDCK cells grown on <100> substrate may be reacting to this surface through altered ECM interactions with the substrate. This suggested to us that the MDCK cells may also respond to these subtle surface features by reorganizing and secreting their ECM. This type of response to changes in adhesive state and mechanical environment has been documented

previously in a broad range of cell types. To determine whether cells were similarly altering ECM protein expression in response to varied substrates, we examined the expression of several ECM inside these cells, including Collagen II, laminin, fibronectin, and collagenase using confocal microscopy and immunofluorescence. In each case we observed an increase in ECM protein expression in MDCK cells cultured on <100> substrates with the most dramatic increase in the expression in collagenase (Figure 4.10, 4.11).

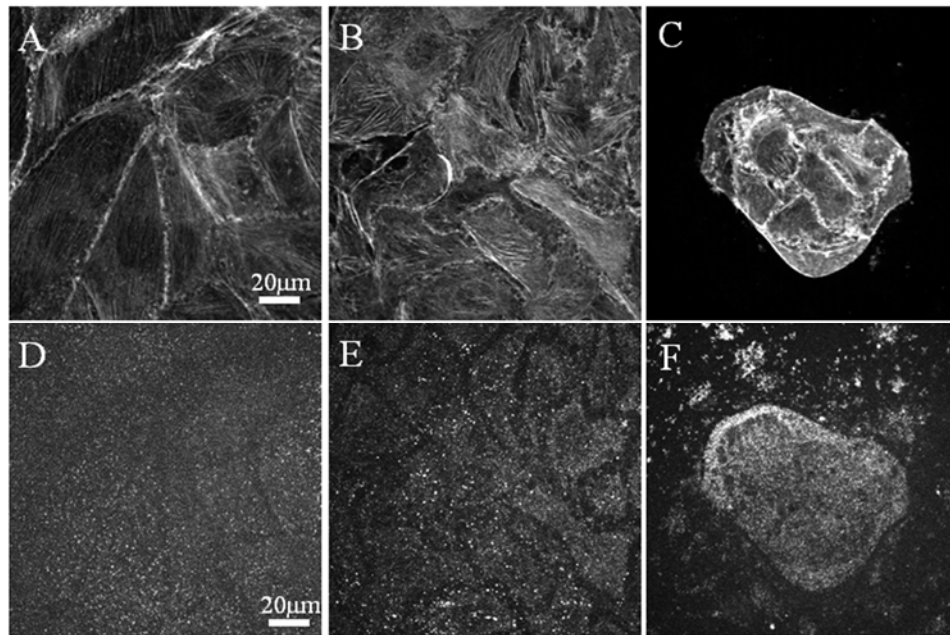


Figure 4.11. Fibronectin Expression in MDCK Epithelial Cells Cultured on GCS, <111> and <100> Substrates.

(A-C) f-actin compared to (D-F) fibronectin organization. Long, well-organized stress fibers can be seen to correlate to consistent and even fibronectin organization.

Although the MDCK cells cultured on $\langle 100 \rangle$ substrates have significantly different morphology, the localization of all the ECM proteins appears as similar punctate structures that are found at the highest concentration on the basal face of the epithelium (Figure 4.11, D-F). The concentration of the punctate ECM laminin deposits is distributed throughout MDCK cells cultured on GCS and $\langle 111 \rangle$ with most of the localization away from the cell outline as defined by actin localization (Figure 4.11 A-C). We observe similar pattern of laminin expression in the cell in MDCK cells cultured on $\langle 100 \rangle$ substrate with the periphery of the clusters have the highest localizations (Figure 4.11 F).

IV.4 Discussion/Conclusion

Nanoscale materials have a great impact on cellular behavior and have been demonstrated to change and control cellular adhesion, proliferation, and differentiation [11, 120]. Even though significant signaling events are invoked when cells are exposed to nanoscale materials [11], a fundamental understanding of the cellular response and the cues to which the cell responds are suggestive. It appears that mechanical and chemical cues are important factors for adhesion and morphology. Many cell-surface interactions are driven through interaction with the extracellular matrix and controlled by its organization and composition [11]. Moreover, the organization of the extracellular matrix is controlled by the external environment as well, which makes it difficult to distinguish between nanoscale material influences that are directly related to cell-

substrate interaction and those influences which are indirectly governed by substrate-ECM interactions [52]. In this study we use a set of substrates that share a common, similar composition – SiO₂, and have only subtle differences in nanoscale structure, approx. 1.5 nm delta Z. Unlike other studies, which use fibroblast cell lines (NIH3T3), transformed cancer cell lines (MCF7), or mesenchymal stem cell lines, we investigated these surfaces with MDCK cells. These cells produce a monolayer epithelium complete with intracellular junctions.

Epithelial cells differ from mesenchymal cells in that they have and require cell-cell interactions for normal function and morphology [18, 139]. Epithelial cells form sheets of cells that are connected physically via adheren junctions, which link the cytoskeleton of one cell to another, adding a level of complexity in regards to mechanical sensing and signaling.

MDCK cells cultured on <100> substrates exhibit strikingly different cuboidal morphology, colony growth habit, and changes to their adhesion based structures, such as actin stress fiber and adherens junction. Although MDCK cell cultured on GSC and <111> grew more similarly, we also observe subtle differences in their behavior and growth habit.

Our results demonstrate that MDCK cells have a robust response to differences in substrate nanotopography and/or surface composition, and that cellular responses may be manifest through a more subtle difference in surface energy. For example, in this study we tested several situations (Figure 4.2) in which distinct surface modifications were present. We found significant

differences between growth rate of MDCK cells cultured on substrates with different crystalline structures, as noted. However, I also found that this effect could be masked by certain surface modifications, such as HMDS coating. As noted previously, topographical variations seem to play a role between GCS and Si Wafer surfaces, while surface chemistry is the dominant factor between crystalline orientations. The one exception was the as-purchased 111 orientation, which showed the highest growth of the group it was tested with. This could be due to the ambient conditions in which the oxide layer grew from the manufacturer, or some other unique characteristic, such as remaining organic material, also from the manufacturer. This work was performed using an epithelial tissue culture cell line to characterization of radical differences in the cellular response to material with similar composition. The results strongly suggest that material properties, other than composition and/or size, must be considered when defining interactions of cells with a substrate, whether it is synthetic or natural.

Protein absorption and cell behavior (growth, adhesion, and modification of the ECM) respond to the crystalline nature of their substrate, which creates small variations in nanotopography. The GCS and <111> silicon wafer showed variations in their surface nanotopography compared to the <100> wafer, which corresponded to increased protein adsorption and cellular growth. An attractive hypothesis emerges from this work. It suggests that small variations, on the order

of 1.5 nm Δz , can significantly alter adsorption kinetics, which is a significant factor behind observed effects.

CHAPTER V

AFM FOR THE INVESTIGATION OF DYNAMIC BIOLOGICAL SYSTEMS

V.1 Introduction

The Atomic Force Microscope (AFM) is a versatile tool that allows sub nanometer imaging resolution and the mapping of physical properties of samples. Unlike light microscopy techniques, the AFM does not suffer from an inherent limitation of resolution due to the wavelength of light; it is more similar to Ion Beam Microscopy, such as the Scanning Electron Microscope (SEM), where electrons have a far shorter wavelength than photons. The Helium Ion Microscope (HIM) is still yet an improvement on the SEM by using a heavier ion than the electron. However, ion beam microscopy has other inherent limitations that the AFM can overcome, such as imaging in physiological conditions, which are aqueous and full of ionic compounds themselves. The inherent resolution limitation of the AFM in either aqueous or non aqueous environments is tip sharpness. Theoretically the AFM can image with a single atom tip, which would allow probes to image the atomic structure of the surface of your sample. Because the AFM does not use ions or other charged particles, it has been widely employed in biological systems, achieving high resolution images of bacteria [140], viruses [141], other microbes [142], and mammalian cells [143], yeast cells [144].

High resolution images are not the only advantage of the AFM. Here, I am interested in mapping the physical properties of samples. Because the AFM uses a cantilever with a sharp tip, it can be modeled as a spring. This allows for various mechanical measurements such as cell elasticity, adhesion forces, and more [145-147].

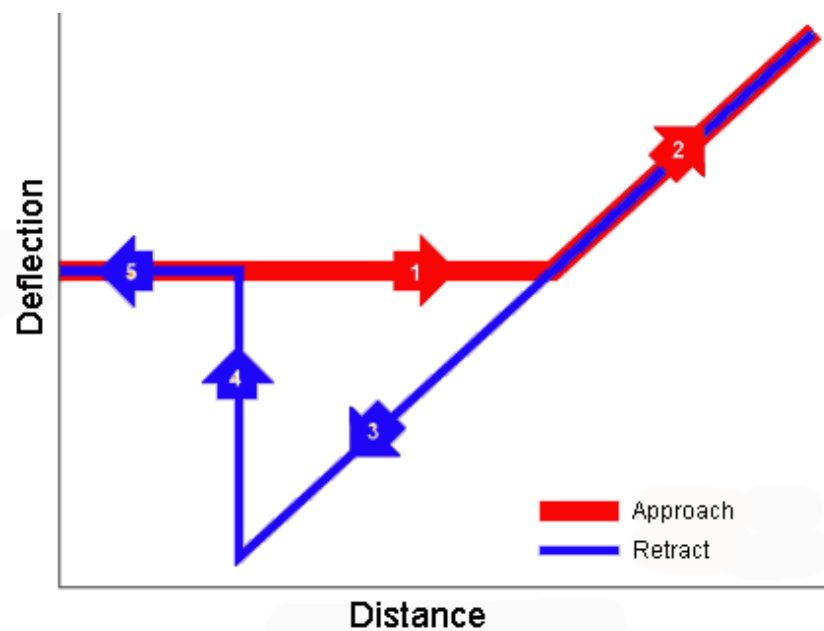


Figure 5.1. Typical Force Distance Curve Using the AFM. The tip approaches the sample from some distance. There is often an attraction regime in which the tip is pulled closer to the sample before coming into contact (not depicted here). This is generally not the case in ionic solutions (such as media) due to an electrostatic double layer that forms on the tip and sample. After the tip makes contact with the sample, it bends in a linear fashion. This is why an AFM cantilever can be modeled as a Hookian spring. The tip is then retracted from the sample and is held to the sample by various adhesion forces before overcoming the forces and snapping back.

The predominate method for achieving this is Force Spectroscopy. This is a simple method in which the tip is brought into contact with the surface and the

deflection is measure with distance the tip travels, this provides a force-distance curve (Figure 5.1). This method has been widely used to probe many different cell types [77, 148-150]. While this technique is easy and reliable, the idea of dynamic mapping and lateral resolution is lacking. This can be partially achieved by using force-volume mapping, which is taking many force-distance curves while imaging [148]. However, this is slow and cannot achieve a dynamic picture of elasticity with high lateral resolution. Force Modulation Microscopy (FMM) is an acoustic method of AFM in which a vertical oscillation is added in contact mode imaging in order to probe the mechanical properties of the cell. Because the actuation frequency of the modulation is far higher than the lateral scan speed, high lateral resolution is achieved [109]. This particular method holds promise as a technique that will allow the dynamic mechanical mapping not achievable with force volume mapping.

V.2 Materials and Methods

Cell Culture: MDCK cells were cultured with DMEM/ High Glucose (Hyclone Cat no. SH30022.01). Cells were transferred using 1x Trypsin/EDTA (MP #1689149) and Cell Striper (Corning REF:25-056-CI). For 25 cm² flasks we used 1.5 milliliters of each for 25 min at 37 degrees C. For 75 cm² we used 3 milliliters of each for 25 min at 37 degrees C. Cells were diluted at 40X for each experiment and were passed between 65-75% confluence.

Surface Preparation: Three specific silicon substrates were used: glass coverslips (GCS; Globe Scientific, Inc., Item #1401-10), <111> crystalline silicon wafer (111-SiW; Ted Pella, Inc., Prod. No. 16010), and <100> crystalline silicon wafer (100-SiW; Ted Pella, Inc., Prod. No. 16015). Surfaces were cleaned with an oxygen plasma cleaner (South Bay Technologies, Inc., PC-2000). Surfaces were washed for 15 min. in Acetone, then 5 min. in Methanol and washed in DI Water. After the initial solvent wash, surfaces were then cleaned with O₂ plasma for 15 min. at 100W.

AFM Imaging: AFM images were obtained using an Agilent 5600 LS AFM. Surfaces were imaged using SiN₄ tips (Ted Pella – SINI-30) with a labeled force constant of 0.2 N/m. Measurements of the spring constant using the thermal-K tool available in Pico View 1.14 (Agilent) software gave values of k within the expected range of 0.2 N/m +- 0.07 N/m. Deflection sensitivities were measured to be 75 nm/V +- 20 nm/V for all experiments. Surfaces were imaged at 1 line/s at 2 nN with a 25 μm² field of view. To help prevent tip contamination, tips were plasma cleaned at 100W for 30 min. and then immersed in methoxy (triethylenoxy) propyltrimethoxy (Gelest, Inc., SIM6493.4) for 24 hours. This was shown to create a monolayer of PEG on silicon nitride surfaces in [151]. Tips were then washed in acetone three times to remove excess polymer. The same tip was used for all images obtain, in a single session (the tips was never removed, only the samples were exchanged).

V.3 Results

Madin-Darby Canine Kidney (MDCK) cells were imaged live using Force Modulation Mode in an AFM on glass cover slips (GCS), and silicon wafers with crystal orientation of $\langle 111 \rangle$ (SiW-111) and $\langle 100 \rangle$ (SiW-100). Deflection images are shown in Figure 5.2. Deflection images can often be thought of as the rate of change in topography. This can provide clear images of features that are missed in purely topographical images. MDCK cells shown in Figure 5.2 show a variety of features; clear intercellular links can be seen on both the GCS and SiW-111 while they appear to be lacking in the SiW-100. Extra cellular space demonstrated more consistent features on GCS and SiW-111 while dispersed patches can be seen on the SiW-100. This could be due to the more favorable affinity of the GCS and SiW-111 demonstrated in protein adsorption assays. FMM amplitude images also showed lower FMM amplitude values in the extracellular matrix space on GCS and SiW-111 compared to SiW-100.

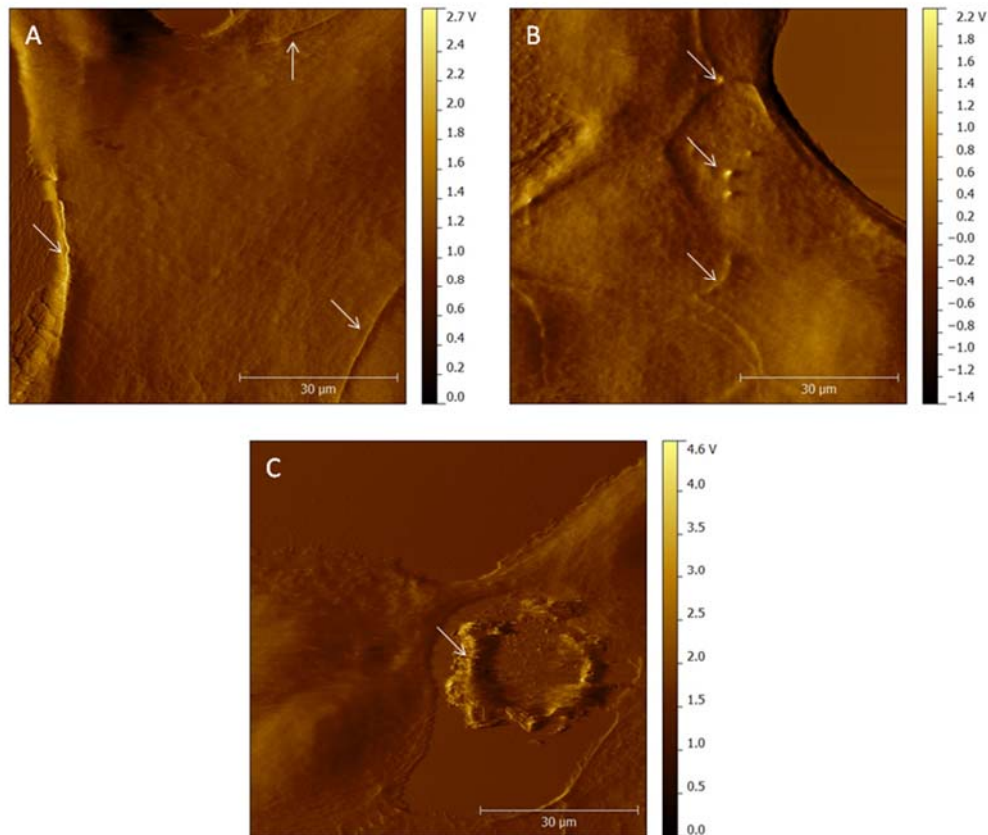


Figure 5.2. Deflection Images of MDCK Cells on Various SiO₂ Substrates. MDCK cells imaged on (A) GCS, (B) SiW-111, and (C) SiW-100. Arrows indicate sharp changes in topography. Clear intercellular boundaries can be seen (arrows) in A and B. Nodules can also be seen in B, which could indicate surface structures such as microvilli. C is a sharp circular mass which could be the remnants of a dead cell.

One of the things FMM AFM may be able to be used for is to dynamically map surface properties to gain an understanding of how live cells may change. FMM could provide a high lateral resolution not attainable in other methods, such as a simple force-distance curve. FMM AFM can also provide superior images of organic thin films, such as block co-polymers, where two different polymers are used. Two different polymers may have two different elastic properties, which

would be distinguishable in both the FMM amplitude image as well as the FMM phase image. It is difficult, however, to parse out all of the information contained in a FMM image. We extracted the profiles of MDCK cells imaged with FMM on GCS (Figure 5.3). Notice that a sharp change in topography is correlated with a sharp change in each different piece of data collected: deflection, FMM amplitude, and FMM phase. This is to be expected between topography and deflection images, as mentioned before, because deflection images can often be thought of as the rate of change in topography. FMM amplitude and FMM phase images are supposed to contain information regarding the mechanical properties of the cell. In such a case, it is impossible to tell the difference between what is topography and what is elasticity without manipulating how the instrument operates [109].

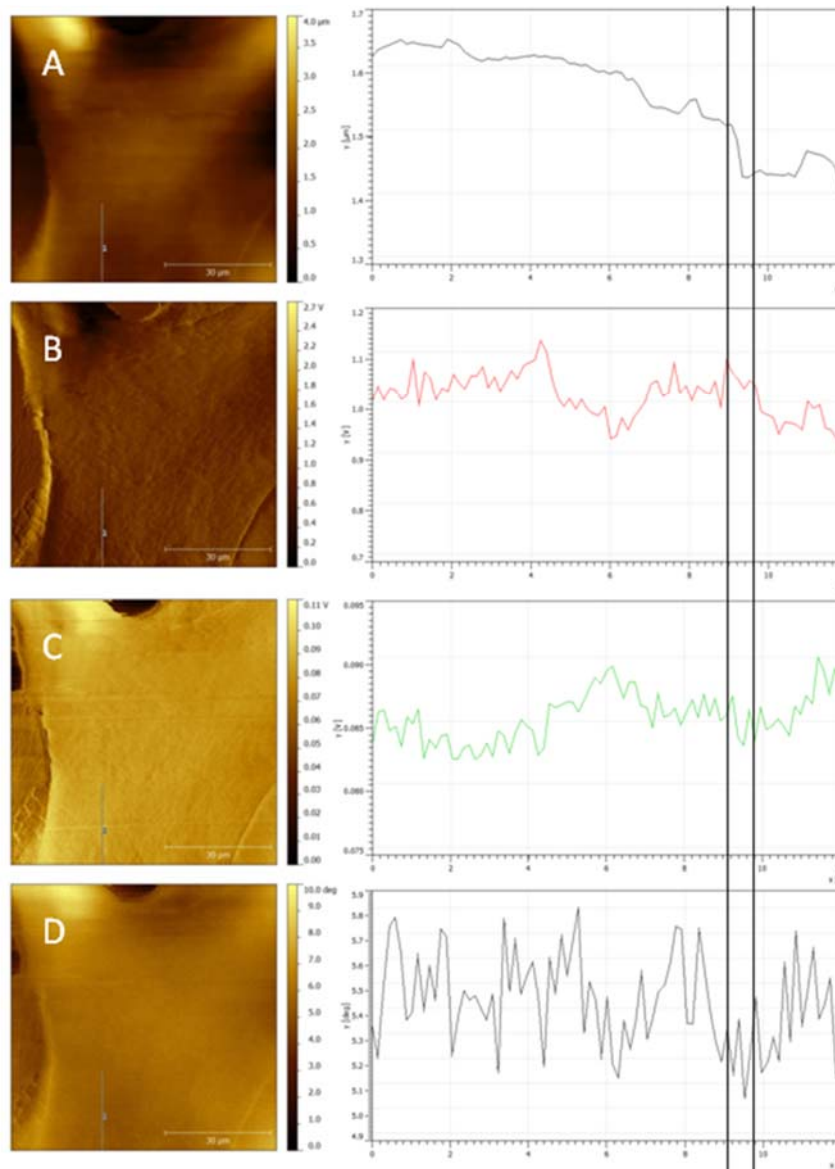


Figure 5.3. Profiles of FMM AFM Image of MDCK Cells on GCS. Profiles of the different sets of data are shown. (A) Topographic, (B) Deflection, (C) FMM Amplitude, and (D) FMM Phase, each with corresponding profile to the right of the main image. Notice the correlation between a change in topography and change in the rest, indicating the difficulty in understanding FMM data.

In order to try and parse out information within the FMM image, single points were taken on relatively flat parts of the cellular membrane. We found a

significant difference between amplitudes on the cell membrane of cells cultured on GCS and SiW-111 compared to SiW-100. We also found a significant difference between amplitudes on and off the cell for cells cultured on GCS and SiW-111, but not for cells cultured on SiW-100.

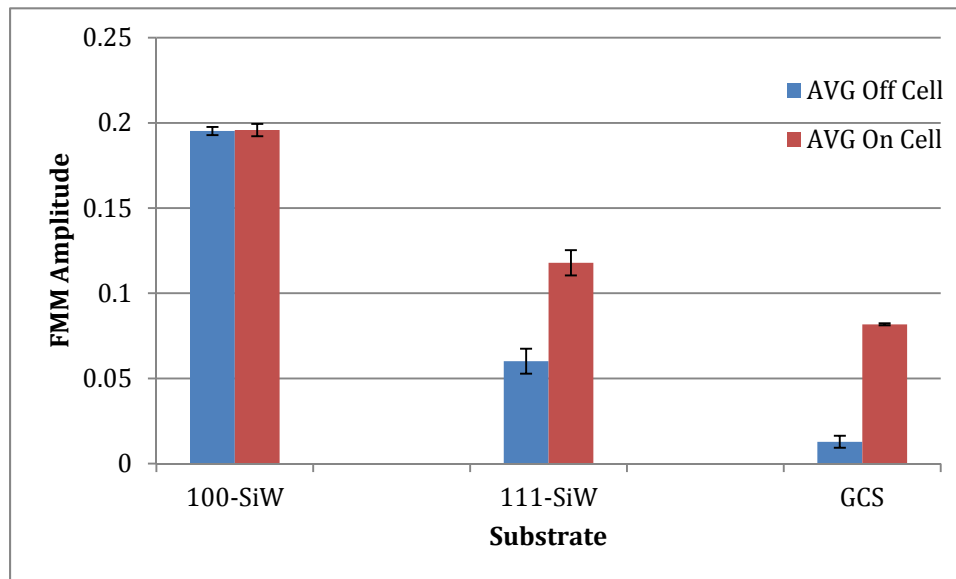


Figure 5.4. FMM Amplitudes On and Off the Cell.

Average amplitudes (n=10) on and off the cell on each substrate. Significant differences were found between each case (substrate compared to substrate, as well as on and off the cell for each substrate), except for the SiW-100 where the FMM amplitude measured on and off the cell were virtually the same. Significance measure as $p < 0.05$.

FMM Amplitudes are correlated with the storage modulus of a material. This is the strain response to a stress. The Young's modulus is a well known example of the constant of proportionality within a linear regime for stress to strain. It is worth noting again that biological materials are not truly elastic materials. It is also a stretch to even talk about a Young's Modulus, because the Young's Modulus is

really only a viable model as an ideal spring. There are several different kinds of modulus however, such as the reduced Young's Modulus, a dynamic modulus, etc. which are used when materials do not quite fit a linear idea. Viscoelastic materials, which biological samples would most be associated with, have two facets, a storage and loss modulus. As the FMM amplitude could be correlated more with the storage modulus, the loss modulus is related to the FMM phase. The phase profiles of cells on each substrate were extracted (Figure 5.5). We note that the variation in phase is greatest on GCS and SiW-111 and variations on the SiW-100 are half as large. This may suggest that the mechanical properties of the cell membrane are more consistent on cells cultured on SiW-100 compared to the other substrates. This could be due to an increase in cortical actin, or up regulated cell-cell adhesion molecules as demonstrated previously.

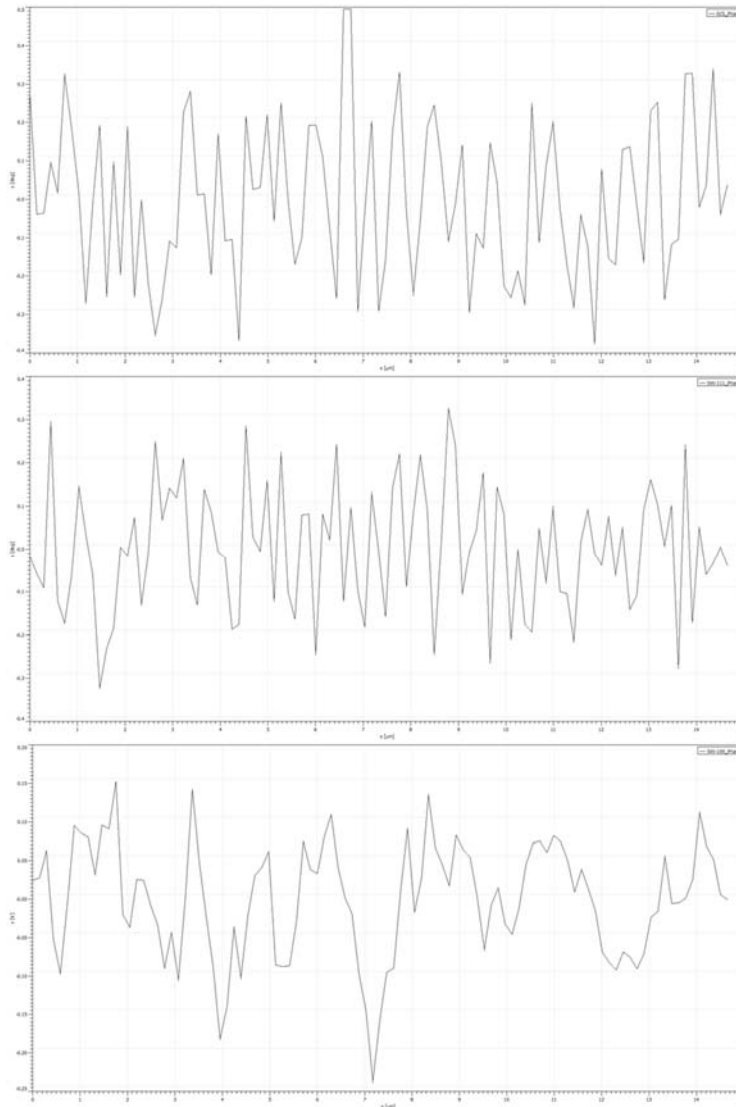


Figure 5.5. Phase Profiles of Each Surface.

Phase profiles are given for each surface: (A) GCS, (B) SiW-111, (C) SiW-100. A and B both have values between 0.3 and -0.3 degrees, while C was measured at a delta half that. C also demonstrated fewer peaks and troughs, which may indicate a lower loss modulus of the membrane. This could be due to differences in how the cell is coping with the unfavorable adhesion noted on the SiW-100, where resources are devoted to increased ECM production. It could also be indicative of a greater amount of cortical actin making the mechanical properties of the membrane more consistent.

V.4 Discussion/Conclusion

FMM AFM is an acoustic method that allows for the mapping of mechanical properties with high lateral resolution. This is in contrast to force-distance curves, which can also measure elastic properties of the cell but do so at a much slower pace and without the high lateral resolution. Here, we've shown that FMM AFM images can be used to image live cells. The tip treatment allowed us to image over a long period of time with no noticeable tip contamination. We obtained FMM AFM images of MDCK cells on three different substrates, GCS, SiW-111, and SiW-100. FMM amplitude varied in a significant manner between GCS and SiW-111 compared to SiW-100 with the later showing larger amplitudes over the cell membrane. There was also a significant difference in amplitude between the cell and substrate, again with the SiW-100 showing the greatest amplitude measured as well as the least difference between substrate and cell. We also extracted the phase profile of cells cultured on each substrate. The data again suggested that cells cultured on the SiW-100 substrates were noticeably different. Cells cultured on the GCS and SiW-111 have phase shifts between 0.3 degrees and -0.3 degrees whereas the SiW-100 demonstrated shifts between 0.15 and -0.15 degrees. This may indicate greater cortical actin compared to the other substrates, or a more uniform cellular membrane as cells cultured on the SiW-100 spend resource to cope with the unfavorable adhesion environment.

We also demonstrated the coupling of topographical changes with change in deflection (as expected), and FMM amplitudes and FMM phase shifts (Figure 5.3). As mentioned before, it is known that there has yet to be a method of deconvoluting topographical changes with FMM amplitude, because FMM amplitudes are measured in the deflection of the cantilever [109]. It is not immediately clear that this is an impossibility, as FMM images could be viewed similar to force-distance volume measurements. FMM images are obtained by putting a vertical oscillation on the cantilever as it scans in contact mode. The position of the cantilever can be determined which allows one to find the spring constant of the cantilever. To find the spring constant of a cantilever, distance traveled is known and plotted against cantilever deflection so that voltage can be correlated to distance travelled. Each oscillation is met with some deflection; as the piezo moves down the cantilever is deflected and the FMM amplitude is measured. When the cantilever is returned to its original position the deflection should return to the desired setpoint. If this is not true, then the cantilever is raised until the setpoint is achieved and the difference can be measured as the deflection, and topographical change recorded. In an attempt to deconvolute topographical changes from FMM amplitude, scanning could be halted at this point until a full oscillation occurs and an appropriate FMM amplitude measurement is achieved. However, this method may in turn eliminate a meaningful phase shift. If oscillations are halted it is unclear what a phase shift means when a topographical change has occurred. The deflection could be

recorded and the FMM amplitude ignored, but again this does not capture the desired mechanical properties, as the data would have missing pieces. The most practical and inexpensive solution would seem to be a two-pass system. For materials that are unchanged over time one could measure topographical information first, and then repeat the path with a vertical oscillation allowing for FMM measurements to be reliably taken. The problem with this method is that biological systems, such as cells, do not stay static over time. This means that a rapid scanning method would have to be employed, which in turn presents a number of problems that AFM faces in many other situations and should be familiar to those interested in the AFM as an analytical instrument. Another possibility is a two-cantilever system, where the first cantilever is in contact mode and guides the second in regards to topographical changes. This system would allow for the rapid mapping of mechanical properties with the high spatial resolution and speed desired. This may pose several engineering problems but seems to be a pragmatic possibility.

CHAPTER VI

CONCLUSION AND GUIDING PRINCIPLES

The adhesion behavior of a model epithelial cell on surfaces with nanoscale variations is subtle, and yet robust. This work demonstrated that **cellular adhesion is sensitive enough to respond to differences in changes such as crystalline orientation and surface chemistry**. Initial results showed that MDCK cells grew favorably on the GCS compared to a Si Wafer (Figure 3.2) with fewer small islands on GCS (Table 3.1) and more visible actin stress fibers (Figure 3.5). AFM images of surface topography demonstrated a slight difference in GCS compared to Si Wafer (Figure 3.1) indicating that variations in nanotopography could be the driving factor. However, further investigation found that the story was more complex. AFM images of GCS compared to Si Wafer of crystalline orientation $\langle 111 \rangle$ and $\langle 100 \rangle$ showed that topography between GCS and $\langle 111 \rangle$ to be very similar, and the surface of the $\langle 100 \rangle$ orientation to be flatter (Figure 4.1). For initial cleaning methods, cells demonstrated preferential growth on both the GCS and $\langle 111 \rangle$. However, **varying cleaning procedures and modifying surface chemistry significantly altered previously observed effects**. As-purchased oxide layers varied cell growth between all three surfaces with the $\langle 100 \rangle$ orientation showing the least number of cells over 4 days (Figure 4.2). Native oxide layers, where the as-purchased oxide layer was stripped and

allowed to regrow, demonstrated a similar trend, again with the <100> orientation showing the lowest cell growth. However, the as-purchased <111> surface had more cells than the GCS control, suggesting that the thickness or structure of the oxide layer from the manufacturer played an important part, or some unknown, uncharacterized organic material remained after the as-purchased wafers were cleaned using a standard RCA-1 cleaning protocol; therefore, **properly controlling how the native oxide layer grows is a requirement for ensuring experimental consistency**. But, the effects observed are not simply due to the morphological differences of surfaces because modifying the surface chemistry eliminated the differences between the <111> and <100> orientation (Figure 4.2). As such, two general trends emerged with GCS to Si Wafer showing variations that could be primarily due to topographical differences and crystalline orientation being dominated by chemical effects. Overall, **these data demonstrate that there is a very tight interplay between chemical and morphological effects where great precision is needed in order to control desired affects**. For example, to attain a more rounded, or cuboidal cell morphology, one may design a very flat topography; such effects were observed on the <100> orientation (Figure 4.4). But, as demonstrated, surface chemistry modifications may nullify such an effect returning the growth behavior to normal.

Data also suggests that the ECM plays a major role in "reading" substrates. Growth and morphological changes on the <100> surface had corresponding protein adsorption levels differences (Figure 4.8). Hence,

topographical variations under a specific size, such as 10 nm, should be carefully characterized in order to understand how protein interactions change. Such sizes are too small to physically alter the cell but affect protein interactions with surfaces.

Variations in adhesion behavior go beyond simply altering cell growth numbers, specific protein adsorption on the surface, or organization within the cell. Physical characteristics of the cell change with various surfaces. Such changes were observed using Force Modulation AFM (Figure 4.5). MDCK cells were imaged on each surface, GCS, $\langle 111 \rangle$ and $\langle 100 \rangle$ Si Wafer. **Cellular stiffness was found to correspond with observed adhesion variations.** For example, the $\langle 100 \rangle$ orientation was found to be nearly twice as stiff as the GCS control or $\langle 111 \rangle$ orientation (Figure 5.4). Also, AFM images also demonstrated variations in phase profiles of cells grown on $\langle 100 \rangle$ compared to GCS and $\langle 111 \rangle$ (Figure 5.5), demonstrated a more consistent cell membrane structure on $\langle 100 \rangle$ compared to GCS and $\langle 111 \rangle$ (Figure 5.5). These data suggest that investigations should go beyond simply examining protein levels, or protein distributions within the cell, and consider the mechanical properties of cells.

Understanding how sensitive a cell's ability to "read" surfaces can be, what reactions cells have, and how it affects physical aspects of the cell, could lead to better designed devices and predictive models. It is slightly surprising that cells are sensitive enough to differentiate surfaces with nearly identical chemical composition but slightly varying surface organization. These results demonstrate

the exquisite sensitivity that biological systems exhibit towards nanoscale physical and chemical interactions. This remains a rich area for investigation.

REFERENCES

1. Adisheshaiah, P., et al., *A novel gadolinium-based trimetasphere metallofullerene for application as a magnetic resonance imaging contrast agent*. Investigative Radiology, 2013. **48**(11): p. 745-754.
2. Bakermans, A.J., et al., *Small animal cardiovascular MR imaging and spectroscopy*. Progress in Nuclear Magnetic Resonance Spectroscopy, 2015. **88-89**: p. 1-47.
3. Olowokure, O. and X. Qi, *Pancreatic cancer: Current standards, working towards a new therapeutic approach*. Expert Review of Anticancer Therapy, 2014. **14**(5): p. 495-497.
4. Dellinger, A., et al., *Application of fullerenes in nanomedicine: An update*. Nanomedicine, 2013. **8**(7): p. 1191-1208.
5. Dellinger, A.L., et al., *Inhibition of inflammatory arthritis using fullerene nanomaterials*. PLoS ONE, 2015. **10**(4).
6. Madhankumar, A.B., et al., *Interleukin-13 receptor-targeted nanovesicles are a potential therapy for glioblastoma multiforme*. Molecular Cancer Therapeutics, 2006. **5**(12): p. 3162-3169.
7. Miyoshi, H. and T. Adachi, *Topography design concept of a tissue engineering scaffold for controlling cell function and fate through actin cytoskeletal modulation*. Tissue Engineering - Part B: Reviews, 2014. **20**(6): p. 609-627.
8. Martino, S., et al., *Stem cell-biomaterial interactions for regenerative medicine*. Biotechnology Advances, 2012. **30**(1): p. 338-351.
9. Kim, D.H., et al., *Matrix nanotopography as a regulator of cell function*. Journal of Cell Biology, 2012. **197**(3): p. 351-360.
10. Ferrari, A., et al., *Nanotopographic Control of Neuronal Polarity*. Nano Letters, 2011. **11**(2): p. 505-511.
11. Anselme, K., et al., *The interaction of cells and bacteria with surfaces structured at the nanometre scale*. Acta Biomaterialia, 2010. **6**(10): p. 3824-3846.
12. Wozniak, M.A., et al., *Focal adhesion regulation of cell behavior*. Biochimica Et Biophysica Acta-Molecular Cell Research, 2004. **1692**(2-3): p. 103-119.
13. Yang, K., et al., *Nanotopographical Manipulation of Focal Adhesion Formation for Enhanced Differentiation of Human Neural Stem Cells*. ACS Applied Materials & Interfaces, 2013. **5**(21): p. 10529-10540.
14. Gonzalez-Garcia, C., et al., *Effect of nanoscale topography on fibronectin adsorption, focal adhesion size and matrix organisation*. Colloids and Surfaces B-Biointerfaces, 2010. **77**(2): p. 181-190.

15. Yu, C.H., et al., *Early integrin binding to Arg-Gly-Asp peptide activates actin polymerization and contractile movement that stimulates outward translocation*. Proceedings of the National Academy of Sciences of the United States of America, 2011. **108**(51): p. 20585-20590.
16. Denis, F.A., et al., *Protein adsorption on model surfaces with controlled nanotopography and chemistry*. Langmuir, 2002. **18**(3): p. 819-828.
17. Hammarin, G., et al., *Enhanced laminin adsorption on nanowires compared to flat surfaces*. Colloids and Surfaces B: Biointerfaces, 2014. **122**: p. 85-89.
18. Alberts, B., et al., *Molecular Biology of the Cell, Fourth Edition*. 2002: Garland Science.
19. Israelachvili, J., *Intermolecular and Surface Forces, Third Edition*. 2010: Academic Press.
20. Humphries, M.J., *Integrin structure*. Biochem Soc Trans, 2000. **28**(4): p. 311-39.
21. Wehrle-Haller, B., *Assembly and disassembly of cell matrix adhesions*. Current Opinion in Cell Biology, 2012. **24**(5): p. 569-581.
22. Eng, E.T., et al., *Intact α IIb β 3 integrin is extended after activation as measured by solution x-ray scattering and electron microscopy*. Journal of Biological Chemistry, 2011. **286**(40): p. 35218-35226.
23. Montanez, E., et al., *Kindlin-2 controls bidirectional signaling of integrins*. Genes and Development, 2008. **22**(10): p. 1325-1330.
24. Holle, A.W. and A.J. Engler, *More than a feeling: discovering, understanding, and influencing mechanosensing pathways*. Current Opinion in Biotechnology, 2011. **22**(5): p. 648-654.
25. DeMali, K.A., X. Sun, and G.A. Bui, *Force transmission at cell-cell and cell-matrix adhesions*. Biochemistry, 2014. **53**(49): p. 7706-7717.
26. Roca-Cusachs, P., T. Iskratsch, and M.P. Sheetz, *Finding the weakest link-exploring integrin-mediated mechanical molecular pathways*. Journal of Cell Science, 2012. **125**(13): p. 3025-3038.
27. Partridge, M.A. and E.E. Marcantonio, *Initiation of attachment and generation of mature focal adhesions by integrin-containing filopodia in cell spreading*. Molecular Biology of the Cell, 2006. **17**(10): p. 4237-4248.
28. Pasapera, A.M., et al., *Myosin II activity regulates vinculin recruitment to focal adhesions through FAK-mediated paxillin phosphorylation*. Journal of Cell Biology, 2010. **188**(6): p. 877-890.
29. Lawson, C. and D.D. Schlaepfer, *Integrin adhesions: Who's on first? What's on second? Connections between FAK and talin*. Cell Adhesion & Migration, 2012. **6**(4): p. 302-306.
30. Nievers, M.G., R.Q.J. Schaapveld, and A. Sonnenberg, *Biology and function of hemidesmosomes*. Matrix Biology, 1999. **18**(1): p. 5-17.
31. Bhatt, T., et al., *Signaling and mechanical roles of E-cadherin*. Cell Communication and Adhesion, 2013. **20**(6): p. 189-199.

32. Drees, F., et al., *α -catenin is a molecular switch that binds E-cadherin- β -catenin and regulates actin-filament assembly*. Cell, 2005. **123**(5): p. 903-915.
33. Yamada, S., et al., *Deconstructing the cadherin-catenin-actin complex*. Cell, 2005. **123**(5): p. 889-901.
34. Braga, V., *Epithelial cell shape: Cadherins and small GTPases*. Experimental Cell Research, 2000. **261**(1): p. 83-90.
35. Thiery, J.P., et al., *Epithelial-Mesenchymal Transitions in Development and Disease*. Cell, 2009. **139**(5): p. 871-890.
36. Cavallaro, U., B. Schaffhauser, and G. Christofori, *Cadherins and the tumour progression: Is it all in a switch?* Cancer Letters, 2002. **176**(2): p. 123-128.
37. Cavallaro, U. and G. Christofori, *Cell adhesion in tumor invasion and metastasis: Loss of the glue is not enough*. Biochimica et Biophysica Acta - Reviews on Cancer, 2001. **1552**(1): p. 39-45.
38. Chen, G., et al., *Actin-myosin contractility is responsible for the reduced viability of dissociated human embryonic stem cells*. Cell Stem Cell, 2010. **7**(2): p. 240-248.
39. Xu, Y., et al., *Revealing a core signaling regulatory mechanism for pluripotent stem cell survival and self-renewal by small molecules*. Proceedings of the National Academy of Sciences of the United States of America, 2010. **107**(18): p. 8129-8134.
40. Fuchs, E. and S. Raghavan, *Getting under the skin of epidermal morphogenesis*. Nature Reviews Genetics, 2002. **3**(3): p. 199-209.
41. Schneider, M.R., et al., *A key role for E-cadherin in intestinal homeostasis and paneth cell maturation*. PLoS ONE, 2010. **5**(12).
42. Tinkle, C.L., et al., *Conditional targeting of E-cadherin in skin: Insights into hyperproliferative and degenerative responses*. Proceedings of the National Academy of Sciences of the United States of America, 2004. **101**(2): p. 552-557.
43. Jamora, C., et al., *Links between signal transduction, transcription and adhesion in epithelial bud development*. Nature, 2003. **422**(6929): p. 317-322.
44. Foote, H.P., K.D. Sumigray, and T. Lechler, *FRAP analysis reveals stabilization of adhesion structures in the epidermis compared to cultured keratinocytes*. PloS one, 2013. **8**(8).
45. Saw, T.B., et al., *Mechanobiology of Collective Cell Migration*. Cellular and Molecular Bioengineering, 2015. **8**(1): p. 3-13.
46. Tse, J.M., et al., *Mechanical compression drives cancer cells toward invasive phenotype*. Proceedings of the National Academy of Sciences of the United States of America, 2012. **109**(3): p. 911-916.
47. Le Duc, Q., et al., *Vinculin potentiates E-cadherin mechanosensing and is recruited to actin-anchored sites within adherens junctions in a myosin II-dependent manner*. Journal of Cell Biology, 2010. **189**(7): p. 1107-1115.

48. Guck, J., et al., *Optical deformability as an inherent cell marker for testing malignant transformation and metastatic competence*. Biophysical Journal, 2005. **88**(5): p. 3689-3698.
49. Deligianni, D.D., et al., *Effect of surface roughness of the titanium alloy Ti-6Al-4V on human bone marrow cell response and on protein adsorption*. Biomaterials, 2001. **22**(11): p. 1241-1251.
50. Keller, T.F., et al., *Facets of protein assembly on nanostructured titanium oxide surfaces*. Acta Biomaterialia, 2013. **9**(3): p. 5810-5820.
51. Yap, F.L. and Y. Zhang, *Protein and cell micropatterning and its integration with micro/nanoparticles assembly*. Biosensors & Bioelectronics, 2007. **22**(6): p. 775-788.
52. Wang, H.J., et al., *Is there an optimal topographical surface in nanoscale affecting protein adsorption and cell behaviors?* Journal of Nanoparticle Research, 2011. **13**(9): p. 4201-4210.
53. Roach, P., D. Farrar, and C.C. Perry, *Interpretation of protein adsorption: Surface-induced conformational changes*. Journal of the American Chemical Society, 2005. **127**(22): p. 8168-8173.
54. Arima, Y. and H. Iwata, *Effect of wettability and surface functional groups on protein adsorption and cell adhesion using well-defined mixed self-assembled monolayers*. Biomaterials, 2007. **28**(20): p. 3074-3082.
55. Wilson, C.J., et al., *Mediation of biomaterial-cell interactions by adsorbed proteins: A review*. Tissue Engineering, 2005. **11**(1-2): p. 1-18.
56. Park, S. and G.I. Im, *Stem cell responses to nanotopography*. Journal of Biomedical Materials Research - Part A, 2015. **103**(3): p. 1238-1245.
57. Uttayarat, P., P.I. Lelkes, and R.J. Composto. *Effect of nano-to micro-scale surface topography on the orientation of endothelial cells*. in *Materials Research Society Symposium Proceedings*. 2005.
58. Yim, E.K.F., et al., *Nanotopography-induced changes in focal adhesions, cytoskeletal organization, and mechanical properties of human mesenchymal stem cells*. Biomaterials, 2010. **31**(6): p. 1299-1306.
59. Bremus-Koebberling, E.A., et al., *Nano structures via laser interference patterning for guided cell growth of neuronal cells*. Journal of Laser Applications, 2012. **24**(4): p. 6.
60. Wijek, J., et al., *Genomic analysis of the role of transcription factor C/EBP delta in the regulation of cell behaviour on nanometric grooves*. Biomaterials, 2013. **34**(8): p. 1967-1979.
61. Yin, Z., et al., *The regulation of tendon stem cell differentiation by the alignment of nanofibers*. Biomaterials, 2010. **31**(8): p. 2163-2175.
62. Dalby, M.J., et al., *In vitro reaction of endothelial cells to polymer demixed nanotopography*. Biomaterials, 2002. **23**(14): p. 2945-2954.
63. Maclaine, S.E., et al., *Optimizing the osteogenicity of nanotopography using block co-polymer phase separation fabrication techniques*. Journal of Orthopaedic Research, 2012. **30**(8): p. 1190-1197.

64. Reynolds, P.M., et al., *Label-Free Segmentation of Co-cultured Cells on a Nanotopographical Gradient*. Nano Letters, 2013. **13**(2): p. 570-576.
65. Dalby, M.J., et al., *Nonadhesive nanotopography: Fibroblast response to poly(n-butyl methacrylate)-poly(styrene) demixed surface features*. Journal of Biomedical Materials Research Part A, 2003. **67A**(3): p. 1025-1032.
66. Riehle, M.O., et al., *Cell behaviour of rat calvaria bone cells on surfaces with random nanometric features*. Materials Science & Engineering C- Biomimetic and Supramolecular Systems, 2003. **23**(3): p. 337-340.
67. Dalby, M.J., et al., *Fibroblast response to a controlled nanoenvironment produced by colloidal lithography*. Journal of Biomedical Materials Research Part A, 2004. **69A**(2): p. 314-322.
68. Berry, C.C., et al., *The fibroblast response to tubes exhibiting internal nanotopography*. Biomaterials, 2005. **26**(24): p. 4985-4992.
69. Dalby, M.J., et al., *Morphological and microarray analysis of human fibroblasts cultured on nanocolumns produced by colloidal lithography*. Eur Cell Mater, 2005. **9**: p. 1-8; discussion 8.
70. Tsimbouri, P.M., et al., *A genomics approach in determining nanotopographical effects on MSC phenotype*. Biomaterials, 2013. **34**(9): p. 2177-2184.
71. Biggs, M.J.P., et al., *Interactions with nanoscale topography: Adhesion quantification and signal transduction in cells of osteogenic and multipotent lineage*. Journal of Biomedical Materials Research Part A, 2009. **91A**(1): p. 195-208.
72. Khang, D., et al., *The role of nanometer and sub-micron surface features on vascular and bone cell adhesion on titanium*. Biomaterials, 2008. **29**(8): p. 970-983.
73. Luo, C., et al., *Modulating cellular behaviors through surface nanoroughness*. Journal of Materials Chemistry, 2012. **22**(31): p. 15654-15664.
74. Lai, M., et al., *Regulation of the behaviors of mesenchymal stem cells by surface nanostructured titanium*. Colloids and Surfaces B-Biointerfaces, 2012. **97**: p. 211-220.
75. Wang, Y., et al., *Biocompatibility of TiO nanotubes with different topographies*. J Biomed Mater Res A, 2013.
76. Zeiger, A.S., B. Hinton, and K.J. Van Vliet, *Why the dish makes a difference: Quantitative comparison of polystyrene culture surfaces*. Acta Biomaterialia, 2013. **9**(7): p. 7354-7361.
77. Gaikwad, R., et al. *Atomic force microscopy helps to develop methods for physical detection of cancerous cells*. in *4th International Conference on Quantum, Nano and Micro Technologies, ICQNM 2010*. 2010.
78. Pal, S., *Design of artificial human joints & organs*. Design of Artificial Human Joints & Organs. Vol. 9781461462552. 2013. 1-419.

79. Tsukruk, V.V., et al., *Probing of micro mechanical properties of compliant polymeric materials*. Journal of Materials Science, 1998. **33**(20): p. 4905-4909.
80. Tsukruk, V.V., et al., *Surface nanomechanical properties of polymer nanocomposite layers*. Langmuir, 2001. **17**(21): p. 6715-6719.
81. Shulha, H., et al., *Some aspects of AFM nanomechanical probing of surface polymer films*. European Polymer Journal, 2004. **40**(5): p. 949-956.
82. Tomasetti, E., R. Legras, and B. Nysten, *Quantitative approach towards the measurement of polypropylene/(ethylene-propylene) copolymer blends surface elastic properties by AFM*. Nanotechnology, 1998. **9**(4): p. 305-315.
83. Krottil, H.U., T. Stifter, and O. Marti, *Lock-in technique for concurrent measurement of adhesion and friction with the scanning force microscope*. Review of Scientific Instruments, 2001. **72**(1 I): p. 150-156.
84. Viani, M.B., et al., *Fast imaging and fast force spectroscopy of single biopolymers with a new atomic force microscope designed for small cantilevers*. Review of Scientific Instruments, 1999. **70**(11): p. 4300-4303.
85. Killgore, J.P., et al., *Quantitative subsurface contact resonance force microscopy of model polymer nanocomposites*. Nanotechnology, 2011. **22**(17).
86. Lahiji, R.R., et al., *Atomic force microscopy characterization of cellulose nanocrystals*. Langmuir, 2010. **26**(6): p. 4480-4488.
87. Bar, G., et al., *Scanning force microscopy study of patterned monolayers of alkanethiols on gold. Importance of tip-sample contact area in interpreting force modulation and friction force microscopy images*. Langmuir, 1997. **13**(3): p. X-377.
88. Drake, B., et al., *Imaging crystals, polymers, and processes in water with the atomic force microscope*. Science, 1989. **243**(4898): p. 1586-1589.
89. Cross, S.E., et al., *Nanomechanical analysis of cells from cancer patients*. Nature Nanotechnology, 2007. **2**(12): p. 780-783.
90. Marti, O., M. Holzwarth, and M. Beil, *Measuring the nanomechanical properties of cancer cells by digital pulsed force mode imaging*. Nanotechnology, 2008. **19**(38).
91. Raman, A., et al., *Mapping nanomechanical properties of live cells using multi-harmonic atomic force microscopy*. Nature Nanotechnology, 2011. **6**(12): p. 809-814.
92. Sato, M., et al., *Local mechanical properties measured by atomic force microscopy for cultured bovine endothelial cells exposed to shear stress*. Journal of Biomechanics, 2000. **33**(1): p. 127-135.
93. Vadillo-Rodríguez, V., et al., *Comparison of atomic force microscopy interaction forces between bacteria and silicon nitride substrata for three commonly used immobilization methods*. Applied and Environmental Microbiology, 2004. **70**(9): p. 5441-5446.

94. Dong, M., S. Husale, and O. Sahin, *Determination of protein structural flexibility by microsecond force spectroscopy*. Nature Nanotechnology, 2009. **4**(8): p. 514-517.
95. Husale, S., H.H.J. Persson, and O. Sahin, *DNA nanomechanics allows direct digital detection of complementary DNA and microRNA targets*. Nature, 2009. **462**(7276): p. 1075-1078.
96. Chang, D.P., et al., *Friction force microscopy of lubricin and hyaluronic acid between hydrophobic and hydrophilic surfaces*. Soft Matter, 2009. **5**(18): p. 3438-3445.
97. Coles, J.M., et al., *Loss of cartilage structure, stiffness, and frictional properties in mice lacking PRG4*. Arthritis and Rheumatism, 2010. **62**(6): p. 1666-1674.
98. Ivanovska, I.L., et al., *Bacteriophage capsids: Tough nanoshells with complex elastic properties*. Proceedings of the National Academy of Sciences of the United States of America, 2004. **101**(20): p. 7600-7605.
99. Jourdan, J.S., et al., *Imaging nanoscopic elasticity of thin film materials by atomic force microscopy: Effects of force modulation frequency and amplitude*. Langmuir, 1999. **15**(19): p. 6495-6504.
100. Radmacher, M., *Studying the Mechanics of Cellular Processes by Atomic Force Microscopy*, in *Methods in Cell Biology*. 2007. p. 347-372.
101. Radmacher, M., R.W. Tillmann, and H.E. Gaub, *Imaging viscoelasticity by force modulation with the atomic force microscope*. Biophysical Journal, 1993. **64**(3): p. 735-742.
102. Yuya, P.A., D.C. Hurley, and J.A. Turner, *Contact-resonance atomic force microscopy for viscoelasticity*. Journal of Applied Physics, 2008. **104**(7).
103. Yuya, P.A., D.C. Hurley, and J.A. Turner, *Relationship between Q-factor and sample damping for contact resonance atomic force microscope measurement of viscoelastic properties*. Journal of Applied Physics, 2011. **109**(11).
104. Killgore, J.P., et al., *Viscoelastic property mapping with contact resonance force microscopy*. Langmuir, 2011. **27**(23): p. 13983-13987.
105. Grierson, D.S., E.E. Flater, and R.W. Carpick, *Accounting for the JKR-DMT transition in adhesion and friction measurements with atomic force microscopy*. Journal of Adhesion Science and Technology, 2005. **19**(3-5): p. 291-311.
106. Johnson, K.L., *Contact Mechanics*. 2003, Cambridge: Cambridge University Press.
107. Syed Asif, S.A., et al., *Quantitative imaging of nanoscale mechanical properties using hybrid nanoindentation and force modulation*. Journal of Applied Physics, 2001. **90**(3): p. 1192-1200.
108. Carpick, R.W., D.F. Ogletree, and M. Salmeron, *A general equation for fitting contact area and friction vs load measurements*. Journal of Colloid and Interface Science, 1999. **211**(2): p. 395-400.

109. Zhang, J., et al., *Mapping mechanical properties of organic thin films by force-modulation microscopy in aqueous media*. Beilstein Journal of Nanotechnology, 2012. **3**(1): p. 464-474.
110. Huey, B.D., *AFM and acoustics: Fast, quantitative nanomechanical mapping*, in *Annual Review of Materials Research*. 2007. p. 351-385.
111. Dalby, M.J., et al., *Rapid fibroblast adhesion to 27nm high polymer demixed nano-topography*. Biomaterials, 2004. **25**(1): p. 77-83.
112. Dalby, M.J., *Cellular response to low adhesion nanotopographies*. Int J Nanomedicine, 2007. **2**(3): p. 373-81.
113. Ferrari, A., et al., *Nanotopographic control of neuronal polarity*. Nano Lett, 2011. **11**(2): p. 505-11.
114. Riboldi, S.A., et al., *Skeletal myogenesis on highly orientated microfibrinous polyesterurethane scaffolds*. Journal of Biomedical Materials Research Part A, 2008. **84A**(4): p. 1094-1101.
115. Hosseini, V., et al., *Engineered Contractile Skeletal Muscle Tissue on a Microgrooved Methacrylated Gelatin Substrate*. Tissue Engineering Part A, 2012. **18**(23-24): p. 2453-2465.
116. Biggs, M.J.P., et al., *The use of nanoscale topography to modulate the dynamics of adhesion formation in primary osteoblasts and ERK/MAPK signalling in STRO-1+enriched skeletal stem cells*. Biomaterials, 2009. **30**(28): p. 5094-5103.
117. Dalby, M.J., et al., *Investigating the limits of filopodial sensing: a brief report using SEM to image the interaction between 10 nm high nano-topography and fibroblast filopodia*. Cell Biology International, 2004. **28**(3): p. 229-236.
118. Dalby, M.J., *Topographically induced direct cell mechanotransduction*. Medical Engineering & Physics, 2005. **27**(9): p. 730-742.
119. Iannone, M., et al., *Nanoengineered surfaces for focal adhesion guidance trigger mesenchymal stem cell self-organization and tenogenesis*. Nano Lett, 2015. **15**(3): p. 1517-25.
120. Lord, M.S., M. Foss, and F. Besenbacher, *Influence of nanoscale surface topography on protein adsorption and cellular response*. Nano Today, 2010. **5**(1): p. 66-78.
121. Gumbiner, B. and K. Simons, *A functional assay for proteins involved in establishing an epithelial occluding barrier: identification of a uvomorulin-like polypeptide*. J Cell Biol, 1986. **102**(2): p. 457-68.
122. Linsenmayer, T.F. and M.J. Hendrix, *Monoclonal antibodies to connective tissue macromolecules: type II collagen*. Biochem Biophys Res Commun, 1980. **92**(2): p. 440-6.
123. Werb, Z., et al., *Signal transduction through the fibronectin receptor induces collagenase and stromelysin gene expression*. J Cell Biol, 1989. **109**(2): p. 877-89.

124. Burton-Wurster, N. and G. Lust, *Molecular and immunologic differences in canine fibronectins from articular cartilage and plasma*. Arch Biochem Biophys, 1989. **269**(1): p. 32-45.
125. Al-Bayati, A.H., et al., *Composition and structure of the native Si oxide by high depth resolution medium energy ion scattering*. Surface Science, 1991. **241**(1-2): p. 91-102.
126. Simoes, M., L.C. Simoes, and M.J. Vieira, *A review of current and emergent biofilm control strategies*. Lwt-Food Science and Technology, 2010. **43**(4): p. 573-583.
127. Dufrêne, Y.F. and A.E. Pelling, *Force nanoscopy of cell mechanics and cell adhesion*. Nanoscale, 2013. **5**(10): p. 4094-4104.
128. Pillet, F., et al., *Uncovering by Atomic Force Microscopy of an original circular structure at the yeast cell surface in response to heat shock*. BMC Biol, 2014. **12**(1): p. 6.
129. Dague, E., et al., *An atomic force microscopy analysis of yeast mutants defective in cell wall architecture*. Yeast, 2010. **27**(8): p. 673-684.
130. Otto, K., *Biophysical approaches to study the dynamic process of bacterial adhesion*. Res Microbiol, 2008. **159**(6): p. 415-22.
131. Wang, D.C., et al., *AFM membrane roughness as a probe to identify oxidative stress-induced cellular apoptosis*. J Biomech, 2011. **44**(16): p. 2790-4.
132. Jin, H., et al., *Apoptosis induction of K562 cells by lymphocytes: An AFM study*. Scanning, 2013. **35**(1): p. 7-11.
133. Hu, M., et al., *Nanostructure and nanomechanics analysis of lymphocyte using AFM: from resting, activated to apoptosis*. J Biomech, 2009. **42**(10): p. 1513-9.
134. Gonnermann, C., et al., *Quantitating membrane bleb stiffness using AFM force spectroscopy and an optical sideview setup*. Integr Biol (Camb), 2015. **7**(3): p. 356-63.
135. Sbaizero, O., et al., *Analysis of long- and short-range contribution to adhesion work in cardiac fibroblasts: an atomic force microscopy study*. Mater Sci Eng C Mater Biol Appl, 2015. **49**: p. 217-24.
136. Twiss, F. and J. de Rooij, *Cadherin mechanotransduction in tissue remodeling*. Cellular and Molecular Life Sciences, 2013. **70**(21): p. 4101-4116.
137. Steinberg, M.S. and M. Takeichi, *Experimental specification of cell sorting, tissue spreading, and specific spatial patterning by quantitative differences in cadherin expression*. Proc Natl Acad Sci U S A, 1994. **91**(1): p. 206-9.
138. Gumbiner, B.M., *Regulation of Cadherin Adhesive Activity*. The Journal of Cell Biology, 2000. **148**(3): p. 399-404.
139. Dukes, J.D., P. Whitley, and A.D. Chalmers, *The MDCK variety pack: choosing the right strain*. BMC Cell Biology, 2011. **12**: p. 4.

140. Eaton, P., et al., *Atomic force microscopy study of the antibacterial effects of chitosans on Escherichia coli and Staphylococcus aureus*. Ultramicroscopy, 2008. **108**(10): p. 1128-1134.
141. Mateu, M.G., *Mechanical properties of viruses analyzed by atomic force microscopy: A virological perspective*. Virus Research, 2012. **168**(1-2): p. 1-22.
142. Dorobantu, L.S., G.G. Goss, and R.E. Burrell, *Atomic force microscopy: A nanoscopic view of microbial cell surfaces*. Micron, 2012. **43**(12): p. 1312-1322.
143. MacKay, J.L. and S. Kumar, *Measuring the elastic properties of living cells with atomic force microscopy indentation*, in *Methods in Molecular Biology*. 2012. p. 313-329.
144. Wang, C., et al., *Morphological and mechanical imaging of Bacillus cereus spore formation at the nanoscale*. Journal of Microscopy, 2015. **258**(1): p. 49-58.
145. Rabinovich, Y., et al., *Atomic force microscopy measurement of the elastic properties of the kidney epithelial cells*. Journal of Colloid and Interface Science, 2005. **285**(1): p. 125-135.
146. Gadegaard, N., *Atomic force microscopy in biology: Technology and techniques*. Biotechnic and Histochemistry, 2006. **81**(2-3): p. 87-97.
147. Variola, F., *Atomic force microscopy in biomaterials surface science*. Physical Chemistry Chemical Physics, 2015. **17**(5): p. 2950-2959.
148. Roduit, C., et al., *Stiffness tomography by atomic force microscopy*. Biophysical Journal, 2009. **97**(2): p. 674-677.
149. Shroff, S.G., D.R. Saner, and R. Lal, *Dynamic micromechanical properties of cultured rat atrial myocytes measured by atomic force microscopy*. American Journal of Physiology - Cell Physiology, 1995. **269**(1 38-1): p. C286-C292.
150. Kuznetsova, T.G., et al., *Atomic force microscopy probing of cell elasticity*. Micron, 2007. **38**(8): p. 824-833.
151. Cerruti, M., et al., *Poly(ethylene glycol) monolayer formation and stability on gold and silicon nitride substrates*. Langmuir, 2008. **24**(19): p. 10646-10653.

APPENDIX A
EXPANDED FIGURE

In an effort to give a more visual representation of Figure 4.2, a bar graph equivalent is provided in this appendix. Each graph title in Figure A1 denotes the surface modification.

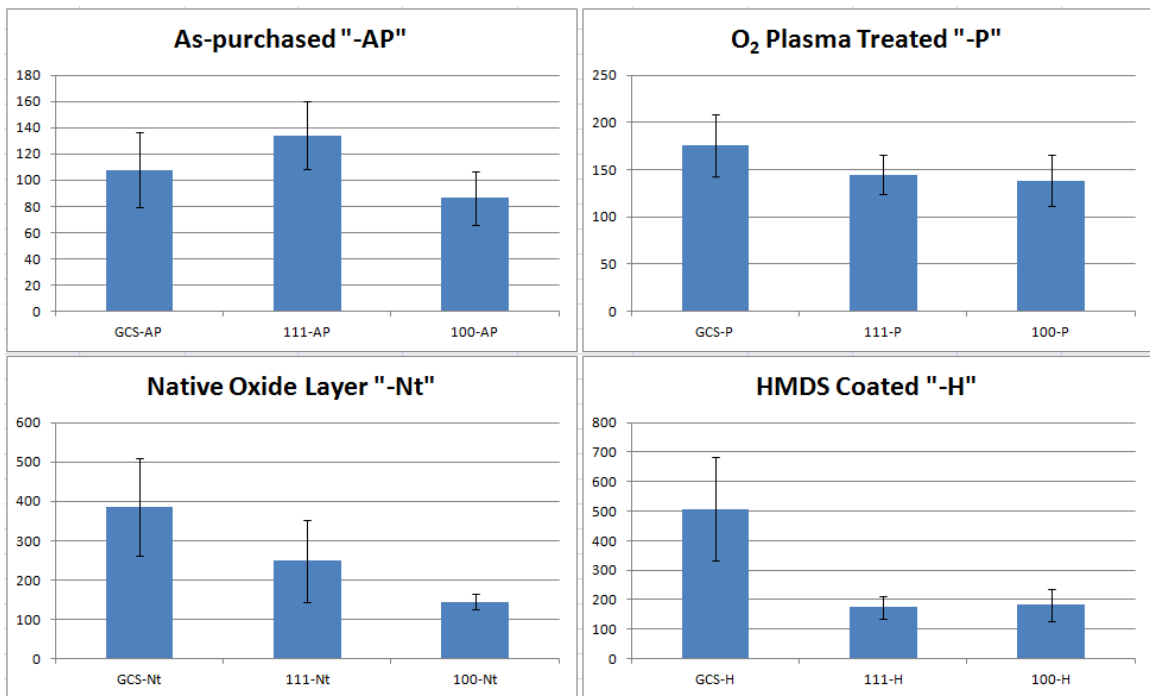


Figure A1. Bar Graph Representation of MDCK Cell Growth Rate. Average number of cells after four days of growth is given for each surface. This bar graph representation of the data in Figure 4.2 demonstrates the general trends between each experimental group. GCS denotes glass coverslip; 111 denotes the Si Wafer of crystalline orientation <111>, and 100 denotes the Si Wafer crystalline orientation <100>.